Article

A transcriptional switch governs fibroblast activation in heart disease

🔴 Check for updates

Michael Alexanian[1], Pawel F. Przytycki[1], Rudi Micheletti[2], Arun Padmanabhan[1,3], Lin Ye[1], Joshua G. Travers[4], Barbara Gonzalez-Teran[1], Ana Catarina Silva[1], Qiming Duan[1], Sanjeev S. Ranade[1], Franco Felix[1], Ricardo Linares-Saldana[5], Li Li[5], Clara Youngna Lee[1], Nandhini Sadagopan[1,3], Angelo Pelonero[1], Yu Huang[1], Gaia Andreoletti[6], Rajan Jain[5], Timothy A. McKinsey[4], Michael G. Rosenfeld[2], Casey A. Gifford[1], Katherine S. Pollard[1,6,7,8,9], Saptarsi M. Haldar[1,3,13 ✉] & Deepak Srivastava[1,10,11,12 ✉]

In diseased organs, stress-activated signalling cascades alter chromatin, thereby triggering maladaptive cell state transitions. Fibroblast activation is a common stress response in tissues that worsens lung, liver, kidney and heart disease, yet its mechanistic basis remains unclear[1,2]. Pharmacological inhibition of bromodomain and extra-terminal domain (BET) proteins alleviates cardiac dysfunction[3–7], providing a tool to interrogate and modulate cardiac cell states as a potential therapeutic approach. Here we use single-cell epigenomic analyses of hearts dynamically exposed to BET inhibitors to reveal a reversible transcriptional switch that underlies the activation of fibroblasts. Resident cardiac fibroblasts demonstrated robust toggling between the quiescent and activated state in a manner directly correlating with BET inhibitor exposure and cardiac function. Single-cell chromatin accessibility revealed previously undescribed DNA elements, the accessibility of which dynamically correlated with cardiac performance. Among the most dynamic elements was an enhancer that regulated the transcription factor MEOX1, which was specifically expressed in activated fibroblasts, occupied putative regulatory elements of a broad fibrotic gene program and was required for TGFβ-induced fibroblast activation. Selective CRISPR inhibition of the single most dynamic *cis*-element within the enhancer blocked TGFβ-induced *Meox1* activation. We identify MEOX1 as a central regulator of fibroblast activation associated with cardiac dysfunction and demonstrate its upregulation after activation of human lung, liver and kidney fibroblasts. The plasticity and specificity of BET-dependent regulation of MEOX1 in tissue fibroblasts provide previously unknown *trans*- and *cis*-targets for treating fibrotic disease.

In many human diseases, dynamic changes in gene expression fuel progressive organ dysfunction. As such, targeting gene transcription has emerged as a new therapeutic strategy in a variety of chronic diseases, including heart failure—a common and lethal condition that affects 24 million people worldwide[8]. Among strategies to therapeutically target the gene regulatory apparatus, small-molecule inhibitors of BET proteins (BRD2, BRD3, BRD4 and BRDT) have emerged as potent tools to reversibly interfere with enhancer-to-promoter signalling in vivo[9]. BET proteins are a highly conserved family of ubiquitously expressed acetyl-lysine reader proteins that co-activate

transcription, and systemic administration of BET bromodomain inhibitors can ameliorate heart failure in mouse models[3,4]. Because the cell types most affected by BET inhibition in these models are not known and systemic administration of potent BET bromodomain inhibitors is likely too broad to be therapeutically tractable for chronic cardiovascular indications, we used single-cell transcriptomic and epigenomic analyses of heart tissue in the setting of intermittent BET bromodomain inhibitor exposure to reveal cell states and *cis*- and *trans*-targets critical for disease pathogenesis and therapeutic efficacy.

[1]Gladstone Institutes, San Francisco, CA, USA. [2]Howard Hughes Medical Institute, Department and School of Medicine, University of California, San Diego, La Jolla, CA, USA. [3]Department of Medicine, Cardiology Division, UCSF School of Medicine, San Francisco, CA, USA. [4]Department of Medicine, Division of Cardiology and Consortium for Fibrosis Research & Translation, University of Colorado Anschutz Medical Campus, Aurora, CO, USA. [5]Cardiovascular Institute and Department of Medicine, Perelman School of Medicine, University of Pennsylvania, Philadelphia, PA, USA. [6]Institute for Computational Health Sciences, University of California, San Francisco, CA, USA. [7]Chan-Zuckerberg Biohub, San Francisco, CA, USA. [8]Department of Epidemiology & Biostatistics, University of California, San Francisco, CA, USA. [9]Institute for Human Genetics, University of California, San Francisco, CA, USA. [10]Department of Pediatrics, UCSF School of Medicine, San Francisco, CA, USA. [11]Roddenberry Center for Stem Cell Biology and Medicine at Gladstone, San Francisco, CA, USA. [12]Department of Biochemistry and Biophysics, University of California, San Francisco, CA, USA. [13]Present address: Amgen Research, Cardiometabolic Disorders, South San Francisco, CA, USA. ✉e-mail: saptarsi.haldar@gladstone.ucsf.edu; deepak.srivastava@gladstone.ucsf.edu
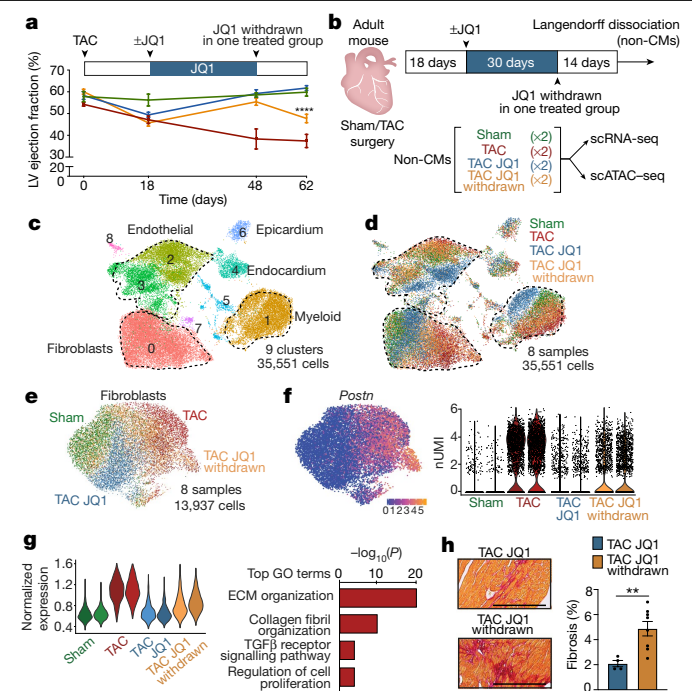
Fig. 1 | Heart failure reversibility with BET inhibition correlates with myofibroblast state. a, Left ventricle (LV) ejection fraction in the indicated groups with treatment and withdrawal of JQ1 (50 mg kg^{-1} per day). ****$P = 1.46 \times 10^{-7}$ for TAC JQ1 versus TAC JQ1 withdrawn at day 62; one-way ANOVA with Tukey post hoc test. Numbers of mice were: sham (green), $n = 4$; TAC (red), $n = 6$; TAC JQ1 (blue), $n = 10$; TAC JQ1 withdrawn (orange), $n = 14$. **b**, scRNA-seq and scATAC-seq library generation workflow. **c**, **d**, Uniform manifold approximation and projection (UMAP) plot of non-cardiomyocytes (non-CMs) captured from hearts in **b** coloured by cluster (**c**) and sample identity (**d**). $n = 35,551$. **e**, UMAP plot of fibroblasts coloured by sample identity, $n = 13,937$. **f**, Fibroblast Periostin (*Postn*) expression shown as UMAP feature and violin plots. nUMI represents the number of unique molecular identifiers associated with the *Postn* gene per cell. **g**, Normalized expression score of the 260 genes increased in TAC versus sham across fibroblast samples and associated GO terms. Fisher's exact test. **h**, Left ventricle fibrosis in TAC JQ1 ($n = 4$) and TAC JQ1 withdrawn ($n = 8$) using Picrosirius red staining and quantification of the fibrosis. **$P = 0.0081$, Mann–Whitney U-test with Tukey post hoc test. Scale bars, 250 μm. **a**, **h**, Data are mean ± s.e.m.

Transcriptional plasticity of fibroblasts

One month of treatment with a small-molecule BET bromodomain inhibitor, JQ1[9], that was started 18 days after the induction of heart failure through left ventricle pressure overload using transverse aortic constriction (TAC), significantly improved left ventricular systolic function in mice (Fig. 1a). Withdrawal of JQ1 for two weeks led to regression of left ventricular systolic function, demonstrating the therapeutic reversibility of BET inhibition. We isolated adult cardiomyocytes and found that the effects of JQ1 on their transcriptome were modest compared with the previously published transcriptomic signature of whole left ventricle tissue (less than 3% overlap)[5] (Extended Data Fig. 1a). To determine the cardiac cell types that are affected by JQ1, we performed single-cell RNA sequencing (scRNA-seq) of more than 35,000 non-cardiomyocytes from four experimental groups using the 10X Genomics platform: sham, TAC vehicle-treated (TAC), TAC JQ1-treated (TAC JQ1), and TAC JQ1-treated followed by JQ1 withdrawal (TAC JQ1 withdrawn) (Fig. 1b). Unsupervised clustering of the scRNA-seq data identified cardiac cell subpopulations, including fibroblasts, endothelial cells, myeloid cells and epicardial cells (Fig. 1c and Extended Data Fig. 1b, c). Among fibroblasts, TAC caused a large shift in cell state, and JQ1 treatment resulted in reversion to a state that closely approached

the sham state (Fig. 1d). Withdrawal of JQ1 shifted the fibroblast population back to a TAC-like stressed state (Fig. 1d). Dynamic JQ1-dependent transcriptomic shifts also occurred in the endothelial and myeloid cell compartments, but cell states elicited by JQ1 were less similar to sham than those elicited in fibroblasts (Fig. 1d and Extended Data Fig. 1d, e).

Subsetting the 13,937 individual fibroblast transcriptomes better illustrated the response to JQ1 in the TAC state (Fig. 1e). Cardiac stress is known to trigger the transition of resident fibroblasts into a contractile and synthetic state called the myofibroblast[10]. Expression of the myofibroblast-enriched gene *Postn*[10], together with many other markers of fibroblast activation, was upregulated in TAC, was downregulated with JQ1 treatment and re-emerged upon JQ1 withdrawal (Fig. 1f and Extended Data Fig. 2a–c). We used a cumulative score to plot expression of 260 fibroblast-associated genes that were upregulated by stress across all samples and found this gene set was highly sensitive to JQ1 exposure (Fig. 1g) and enriched for extracellular matrix (ECM), TGFβ signalling and proliferative gene ontology (GO) terms (Fig. 1g). Differential expression analysis between TAC and TAC JQ1 or TAC JQ1 and TAC JQ1 withdrawn among these 260 genes demonstrated that 81% were significantly downregulated by JQ1, and 38% of those were upregulated again when JQ1 was withdrawn, highlighting the transcriptional reversibility of the stress-induced signature with BET inhibition (Extended Data Fig. 2d). Consistent with transcriptomic data, JQ1 withdrawal led to increased left ventricle fibrosis (Fig. 1h), which may reflect shifts in fibroblast state that influence or are affected by other cell types through heterotypic interactions or paracrine factors. JQ1 exposure also restored expression of a fraction of downregulated genes between sham and TAC in fibroblasts (Extended Data Fig. 2e, f), which suggests that JQ1 has a dual effect by suppressing stress-induced gene programs and restoring basal gene programs. Among the nine fibroblast subclusters, JQ1-treated fibroblasts (cluster 1) were closest to sham (clusters 0, 4) by hierarchical analysis (Extended Data Fig. 3a–c). Although most of the JQ1-withdrawn cells clustered together with TAC cells in the three subclusters associated with the greatest ECM upregulation (clusters 2, 3, 5) (Extended Data Fig. 3d–f), some clustered with sham, which suggests that they achieved stable restoration of gene expression, at least for two weeks after drug withdrawal (Extended Data Fig. 3a–c).

Enhancers during fibroblast activation

To analyse the changes in chromatin accessibility and enhancer activation modulated by JQ1 in non-cardiomyocytes during heart failure pathogenesis, we integrated scRNA-seq data with data from single-cell assay for transposase-accessible chromatin sequencing (scATAC-seq) from the same hearts[11,12] (Fig. 1b and Extended Data Fig. 4a). We identified 490,020 accessible sites distributed among 31,766 individual cells and assigned cellular identity based on chromatin signature (Extended Data Fig. 4b, c). To focus on distal regulatory elements, we excluded accessible sites in promoters and gene bodies and defined a catalogue of fibroblast-, myeloid-cell- or endothelial-cell-enriched distal elements that were used for all subsequent analyses (Extended Data Fig. 4d). Fibroblasts had increased chromatin accessibility after TAC that was reversibly attenuated with JQ1 treatment, a feature that was less evident in myeloid and endothelial cells (Extended Data Fig. 5a). To dissect the dynamic and reversible changes in chromatin activation, we defined open and closed distal elements across the four samples and excluded regions that were constitutively open across all conditions (Extended Data Fig. 5b). We discovered a cluster of highly dynamic distal elements in fibroblasts that were closed in sham, opened in TAC, closed by JQ1, and robustly re-accessible after JQ1 withdrawal (cluster 2) (Extended Data Fig. 5b). GO analysis showed that these regions were proximal to genes controlling heart growth and ECM organization—two hallmark features of adverse cardiac remodelling and fibrosis. We also identified a large cluster of regions in fibroblasts that opened from sham to TAC that were insensitive to JQ1, highlighting a signature of

stress-responsive chromatin activation that is BET-independent (cluster 9) (Extended Data Fig. 5b). In fibroblasts, transcription-factor binding motifs for CEBPB, JUN and MEOX1 were enriched in accessible regions in the sham-to-TAC transition, with subsequent loss of enrichment upon BET inhibition that was then re-acquired with JQ1 withdrawal (Extended Data Fig. 5c).

To identify functionally relevant enhancers among the scATAC-seq peaks, we performed precision nuclear run-on sequencing (PRO-seq)[13] on cultured cardiac fibroblasts in vitro to map genome-wide nascent transcription of RNA polymerase II, which robustly indicates enhancer activity[14] and gene transcription. As PRO-seq requires large quantities of cells, we generated an immortalized cell line derived from primary adult mouse cardiac fibroblasts and treated the cells with TGFβ, a canonical stimulus for eliciting fibroblast activation in vitro (Extended Data Fig. 6a). Induction of *Postn*, *Ctgf* (also known as *Ccn2*) and several other markers validated that this cell line transitioned to the activated state after exposure to TGFβ (Extended Data Fig. 6b). PRO-seq identified a set of distal and gene elements that was significantly more transcribed after TGFβ stimulation and was associated with fibroblast activation (Fig. 2a and Extended Data Fig. 6c–f). Using our scATAC-seq data, we identified distal elements that were either opening or closing between sham and TAC in vivo, and assessed the PRO-seq signal in the cardiac fibroblasts at these same regions. We found that TGFβ-stimulated transcription at distal elements in vitro correlated with regions of chromatin that open in fibroblasts in vivo during heart failure pathogenesis, whereas nascent transcription at chromatin regions that closed in vivo was not notably altered (Fig. 2b and Extended Data Fig. 6g for protein-coding genes). Visualization of the *Postn* locus illustrates this dynamic regulation (Fig. 2c), in which there is chromatin opening in vivo after TAC with dynamic sensitivity to JQ1 exposure. A scATAC-seq co-accessibility analysis between the *Postn* promoter and a TGFβ-dependent region within this area (peak 10/11) showed low co-accessibility in the sham state, a robust increase with TAC, and modulation with JQ1 exposure (Fig. 2c and Extended Data Fig. 6h). We used CRISPR interference (CRISPRi) comprising a catalytically inactive Cas9 (dCas9) fused to the KRAB repressor protein[15] to specifically inhibit individual regulatory elements within this large *Postn* enhancer (Fig. 2d and Extended Data Fig. 6i, j). The peak 10/11 *cis*-element was uniquely required for *Postn* transactivation upon TGFβ stimulation (Fig. 2d). CRISPRi-mediated deposition of the repressive histone mark H3K9me3 was specific to the peak 10/11 region and did not affect the *Postn* promoter (Extended Data Fig. 6k).

Chromatin state and cardiac function

To reveal distal elements involved in progression and reversal of heart failure, we assembled a catalogue of cell-population-enriched large enhancers (also known as super-enhancers)[16] using scATAC-seq data in the diseased heart (TAC) (Extended Data Fig. 7a) and correlated the degree of accessibility of these enhancers in fibroblasts, myeloid cells and endothelial cells with left ventricle ejection fraction in each treatment setting described. This correlation analysis between a measure of enhancer chromatin accessibility and a physiological trait (left ventricle ejection fraction) is summarized schematically in Fig. 2e. Enhancer elements were defined as having a negative correlation if their accessibility was anti-correlated with heart function (that is, opening from sham to TAC) or a positive correlation if closing from sham to TAC. Of the 470 fibroblast super-enhancers identified, 48 showed a strong negative correlation whereas 22 showed strong positive correlation (volcano plot in Fig. 2f and Extended Data Fig. 7b, c). To determine whether the super-enhancers responded similarly in the TGFβ-responsive fibroblast cell line, we performed chromatin immunoprecipitation followed by sequencing (ChIP–seq) with an antibody against H3K27ac, an active enhancer mark, with or without TGFβ-treatment (Extended Data Fig. 7d). Enhancers identified in vivo characterized by a negative correlation with heart function showed increased H3K27ac deposition
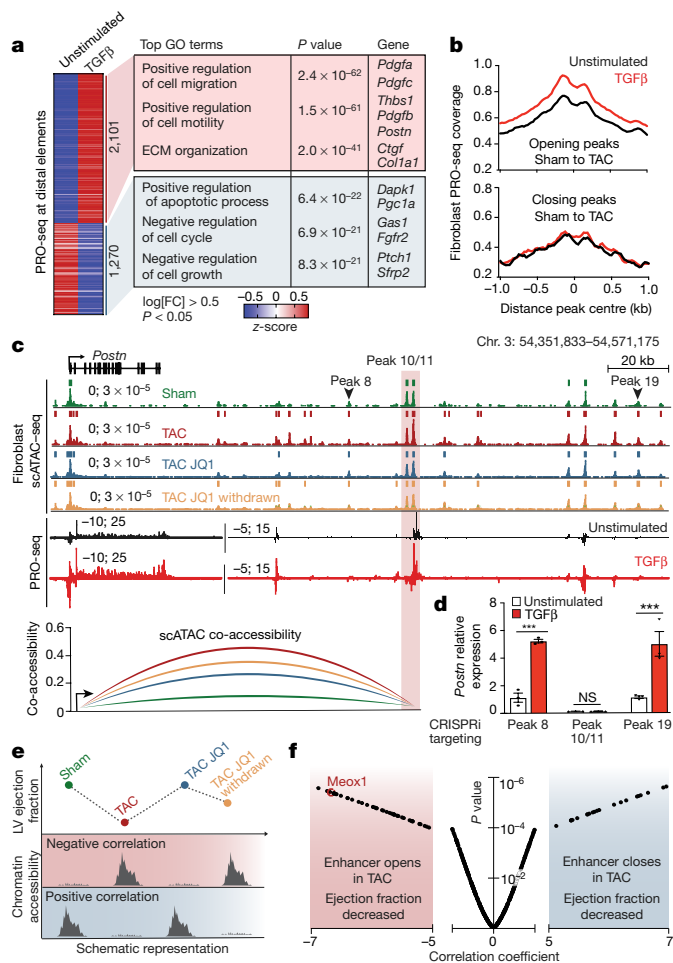

Fig. 2 | Reversibility of chromatin states in fibroblasts reveals DNA elements that correlate with heart function. a, PRO-seq heat map of differentially transcribed distal regions (Wald test with Benjamini–Hochberg correction) in unstimulated versus TGFβ-treated fibroblasts and associated top GO terms (binomial test). The mean signal for two replicates is shown. *Pgc1a* is also known as *Ppargc1a*. **b**, PRO-seq coverage in unstimulated and TGFβ-treated fibroblasts in vitro of scATAC-seq peaks opening (2,553) or closing (567) between sham and TAC in fibroblasts in vivo. **c**, scATAC-seq from fibroblasts in vivo and PRO-seq at the *Postn* locus. A highly transcribed region (peak 10/11) is highlighted with co-accessibility between the *Postn* promoter and peak 10/11. The numbers over the tracks indicate ranges of normalized tag densities. **d**, *Postn* expression by qPCR in unstimulated or TGFβ-treated fibroblasts in CRISPRi lines targeting peak 8 (***P = 0.0001), peak 10/11 or peak 19 (***P = 0.0001). NS, not significant; one-way ANOVA followed by Tukey post hoc test. Values normalized to the CRISPRi control line under unstimulated conditions (shown in Extended Data Fig. 6i). Data are mean ± s.e.m. **e**, Schematic of the correlation analysis between left ventricle ejection fraction and chromatin accessibility highlighting a negative or positive correlation. **f**, Volcano plot showing correlation coefficients (from analysis in Fig. 2e) and corresponding P values of 470 super-enhancers in fibroblasts. See Supplementary Methods for details.

after TGFβ treatment, whereas those with a positive correlation showed decreased H3K27ac (Extended Data Fig. 7e).

One of the most negatively correlated elements in fibroblasts in vivo was a large enhancer downstream of *Meox1* (Fig. 2f and Extended Data Fig. 8a), a homeodomain-containing transcription factor that is required for sclerotome development[17]. *Meox1* was highly upregulated in myofibroblasts after TAC[18] (Fig. 3a and Extended Data Fig. 8b). JQ1 exposure abolished *Meox1* expression, whereas JQ1 withdrawal led to its robust re-induction (Fig. 3a).
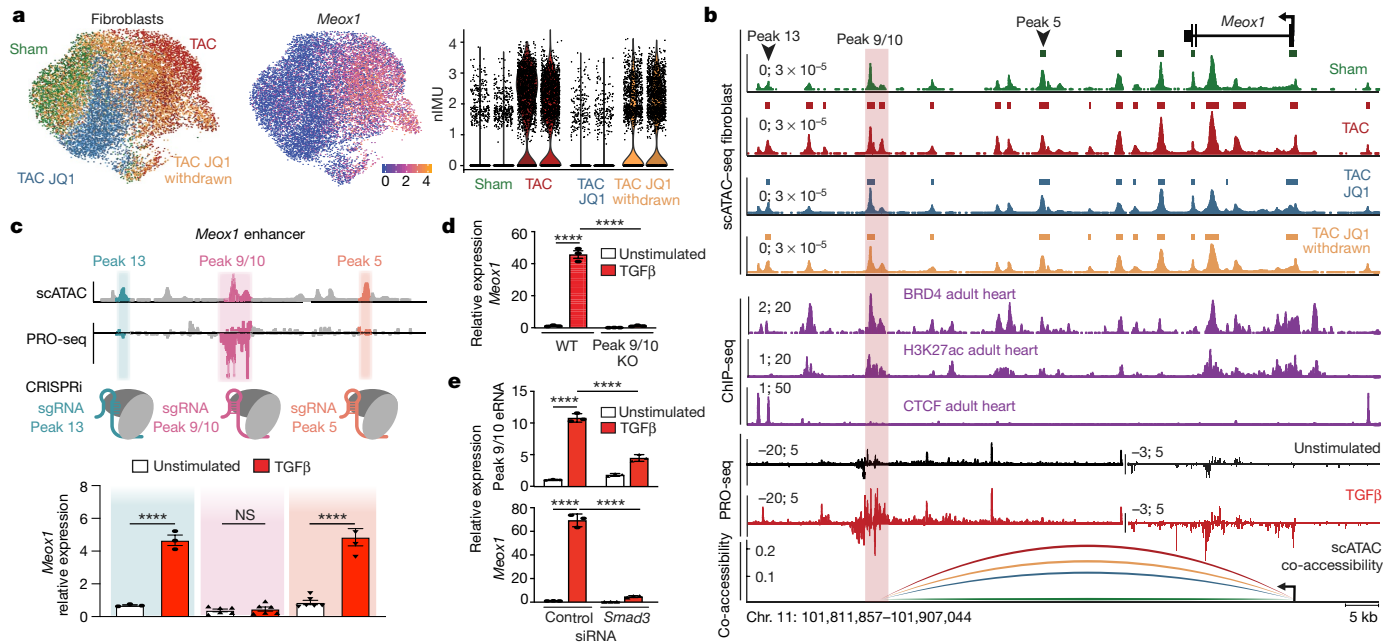
Fig. 3 | Chromatin accessibility and nascent transcription identify a cis-element controlling Meox1 expression. a, UMAP plot of fibroblasts coloured by sample identity or *Meox1* expression with associated violin plots. **b**, Mouse *Meox1* locus showing from top to bottom: scATAC-seq from fibroblasts in vivo; ChIP–seq for BRD4 (GSE46668), H3K27ac and CTCF (ENCSR000CDF and ENCSR000CBI) in the adult heart; coverage of PRO-seq in unstimulated and TGFβ-treated fibroblasts in vitro; and co-accessibility measures between *Meox1* promoter and peak 9 region in fibroblasts. A highly transcribed region (peak 9/10) is highlighted. The numbers over the tracks indicate ranges of normalized tag densities. **c**, Schematic showing CRISPRi targeting of three regions within the *Meox1* enhancer (top). *Meox1* expression

by qPCR in unstimulated or TGFβ-treated fibroblasts upon CRISPRi targeting peak 5 (****$P = 1.82 \times 10^{-10}$), peak 9/10 or peak 13 (****$P = 1.64 \times 10^{-8}$). Values normalized to CRISPRi control line under unstimulated conditions (Extended Data Fig. 10e). **d**, *Meox1* expression by qPCR in unstimulated or TGFβ conditions in wild-type (WT) (****$P = 1.99 \times 10^{-8}$) or peak-9/10-deleted (KO) cells (****$P = 1.99 \times 10^{-8}$). **e**, Expression of peak 9/10 enhancer RNA (eRNA) (top, ****$P = 1.76 \times 10^{-8}$ and ****$P = 5.29 \times 10^{-6}$) and *Meox1* (bottom, ****$P = 9.80 \times 10^{-9}$ and ****$P = 1.29 \times 10^{-8}$) expression by qPCR in unstimulated and TGFβ conditions with control or *Smad3*-targeting siRNAs. **c–e**, Data are mean ± s.e.m. One-way ANOVA followed by Tukey post hoc test.

Stress-induced *cis*-regulation of Meox1

The enhancer downstream of *Meox1* was extremely sensitive to stress and JQ1 exposure in fibroblasts, but not in myeloid and endothelial cells (Fig. 3b and Extended Data Fig. 8c). From sham to TAC conditions, 10 peaks became accessible in fibroblasts; many of these closed with JQ1 treatment back to a sham level, and re-opened when JQ1 was withdrawn (Fig. 3b and Extended Data Fig. 8c–e). Publicly available BRD4 and H3K27ac ChIP–seq data from adult mouse left ventricle tissue corroborated these active enhancer marks at the *Meox1* locus, suggesting that this enhancer may regulate *Meox1* (Fig. 3b). Consistent with BRD4 regulation of this enhancer, activation of *Meox1* mRNA expression induced by TGFβ in cultured fibroblasts[19] was suppressed by JQ1 (Extended Data Fig. 9a), and, among BET proteins, was most sensitive to BRD4 dosage (Extended Data Fig. 9b, c).

Among the scATAC-seq peaks in this locus that showed increased accessibility with TAC in vivo, PRO-seq identified a region located 62–65 kilobases (kb) downstream of the *Meox1* promoter (peak 9/10) that featured a marked increase in nascent transcription after TGFβ stimulation (Fig. 3b). This DNA element showed more TGFβ-stimulated transcription than the *Meox1* gene body itself and was one of the most differentially transcribed regions across the whole genome in response to TGFβ (Fig. 3b and Extended Data Fig. 10a), suggesting a functionally relevant enhancer[14]. The *Meox1* promoter and the peak 9/10 region showed low co-accessibility in the sham state, a strong increase in co-accessibility with TAC, and modulation of co-accessibility with BET inhibition (Fig. 3b and Extended Data Fig. 10b). Chromosome conformation capture analysis of this locus in fibroblasts revealed a robust increase in contact between the peak 9/10 region and the *Meox1* promoter in response to TGFβ (Extended Data Fig. 10c, d). CRISPRi

revealed that the peak 9/10 *cis*-element was specifically required for *Meox1* transactivation upon TGFβ stimulation, while other accessible regions identified in vivo were not (Fig. 3c and Extended Data Fig. 10e, f). Guide RNAs targeting peak 9/10 led to the localized deposition of the repressive H3K9me3 mark in the peak 9/10 element but not on the *Meox1* promoter, supporting specificity of peak 9/10 silencing (Extended Data Fig. 10g). CRISPR–Cas9-based excision revealed that deletion of peak 9/10 abolished *Meox1* transactivation upon TGFβ stimulation (Fig. 3d and Extended Data Fig. 10h). Multiple motifs of SMAD2 and SMAD3, transcriptional mediators of TGFβ signalling, were present in both peak 9/10 and the *Meox1* promoter (Extended Data Fig. 10i), and knockdown of *Smad3*, but not *Smad2*, led to a significant reduction in peak 9/10 transcription and *Meox1* expression (Fig. 3e and Extended Data Fig. 10j,k). Thus, peak 9/10 represents a stress-activated enhancer for *Meox1* during the activated myofibroblast transition.

MEOX1 regulates pro-fibrotic function

Meox1 knockdown reduced the formation of α-smooth muscle (αSMA)-positive stress fibres and expression of *Acta2* (which encodes αSMA) in TGFβ-treated fibroblasts (Extended Data Fig. 11a–d). Moreover, *Meox1* depletion attenuated TGFβ-stimulated collagen-gel contraction and EdU incorporation, two functional hallmarks of myofibroblasts in disease pathogenesis (Fig. 4a and Extended Data Fig. 11e). MEOX1 occupancy by ChIP–seq at active chromatin (marked by H3K27ac) revealed increased recruitment of MEOX1 at stress-responsive distal elements after TGFβ treatment (Fig. 4b and Extended Data Fig. 11f–h). Upon *Meox1* knockdown, transcription of the stress-responsive distal elements bound by MEOX1 in TGFβ-treated fibroblasts—detected
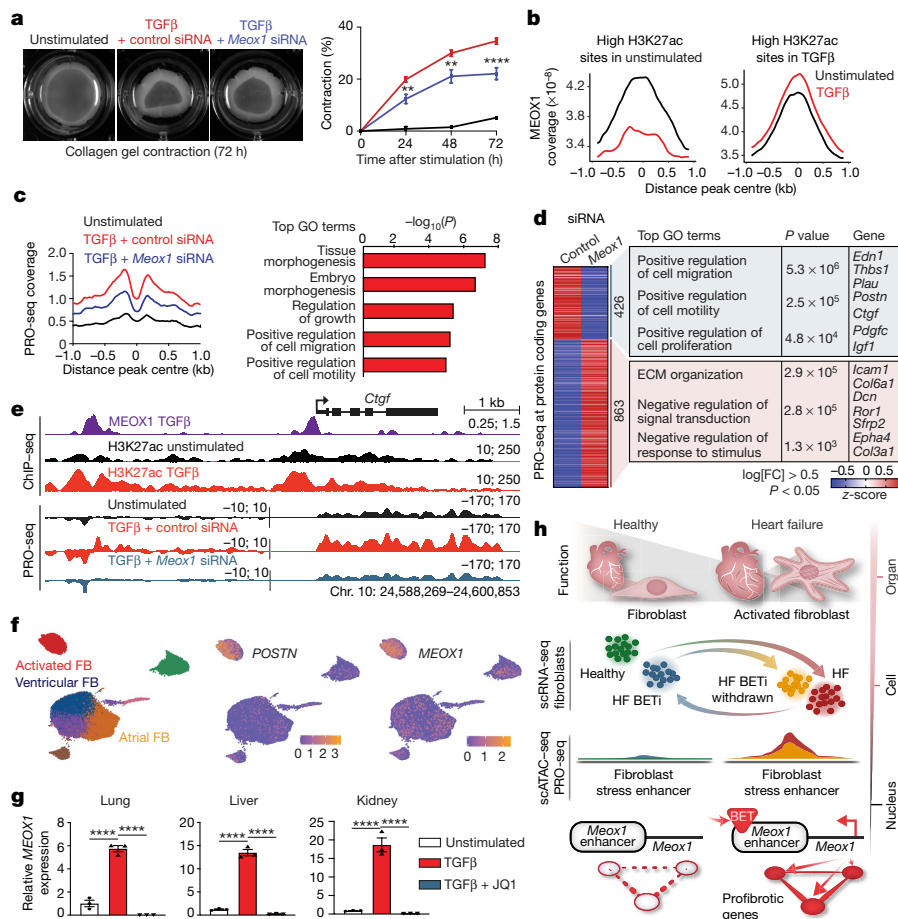
Fig. 4 | MEOX1 regulates fibroblast plasticity and profibrotic function.
a, Images and quantification ($n = 4$ per condition) of fibroblasts seeded on compressible collagen gel matrices in unstimulated or TGFβ conditions with a control or a *Meox1*-targeting siRNA. Two-way ANOVA followed by Bonferroni correction for TGFβ and control siRNA versus TGFβ and *Meox1* siRNA. **$P = 0.0082$ (24 h), **$P = 0.0015$ (48 h) and ****$P = 2.21 \times 10^{-5}$ (72 h). **b**, MEOX1 ChIP–seq coverage in unstimulated and TGFβ-treated cells at distal elements identified by high enrichment of H3K27ac in unstimulated (left, 2,194 regions) or TGFβ-treated (right, 2,898 regions) cells. **c**, Left, PRO-seq coverage under indicated conditions at distal elements with high H3K27ac enrichment in TGFβ versus unstimulated bound by MEOX1 (427 regions) and associated top GO terms (binomial test) (right). **d**, PRO-seq coverage of differentially transcribed genes (Wald test with Benjamini–Hochberg correction) in TGFβ-treated fibroblasts with control or *Meox1* siRNA and associated top GO terms (Fisher exact test). Mean signal for 2 replicates shown. **e**. Coverage of indicated ChIP–seq or PRO-seq with or without TGFβ in cardiac fibroblasts at the *Ctgf* locus with control or *Meox1* siRNA. The numbers over the tracks indicate ranges of normalized tag densities. **f**, UMAP plot of adult human cardiac fibroblasts (FB) coloured by cluster identity (left) and *POSTN* or *MEOX1* expression (right)[20]. **g**, *MEOX1* expression by qPCR in primary human fibroblasts from the indicated tissues. One-way ANOVA followed by Tukey post hoc test for unstimulated versus TGFβ (lung, ****$P = 1.29 \times 10^{-5}$; liver, ****$P = 1.49 \times 10^{-6}$; kidney, ****$P = 5.83 \times 10^{-5}$) and TGFβ versus TGFβ + JQ1 (lung, ****$P = 3.91 \times 10^{-6}$; lung, ****$P = 1.06 \times 10^{-6}$; kidney, ****$P = 4.54 \times 10^{-5}$ kidney). **h**, Model of stress-induced activation of fibroblasts regulated by *Meox1*. BETi, BET inhibition; HF, heart failure. **a**, **g**, Data are mean ± s.e.m.

by PRO-seq—was decreased (Fig. 4c and Extended Data Fig. 11i–k). These distal chromatin loci were near genes linked to tissue morphogenesis, regulation of growth and positive regulation of cell migration and motility (Fig. 4c). Correspondingly, *Meox1* knockdown in the setting of TGFβ stimulation resulted in downregulation of more than 400 genes compared to TGFβ alone, whereas 863 were more highly transcribed (Fig. 4d and Extended Data Fig. 11l–o). GO analysis of the *Meox1*-dependent genes again revealed enrichment of processes associated with fibroblast activation, such as regulation of cell migration, motility and proliferation (Fig. 4d). Among these genes were classic markers of cardiac myofibroblast activation, including *Ctgf* and *Postn*, which showed MEOX1 enrichment at their promoters and proximal regulatory elements (including the *Postn* peak 10/11 enhancer described in Fig. 2c, d). These elements also showed decreased transcription after *Meox1* depletion (Fig. 4e and Extended Data Fig. 11p). Thus, MEOX1 functions as an essential transcriptional mediator of the fibroblast-to-myofibroblast switch associated with fibrotic disease.

MEOX1 is upregulated in human fibrosis

Single-cell data from the human adult heart[20] showed that *MEOX1* was expressed in activated fibroblasts and—together with *POSTN*—was one of the top genes determining the cluster of activated fibroblasts (Fig. 4f and Extended Data Fig. 12a). An atlas of chromatin accessibility from the human fetal heart[21] indicated that the syntenic region of peak 9/10 was characterized by the strongest signal of accessible chromatin in the *MEOX1* distal element in fibroblasts (Extended Data Fig. 12b). Similar to our findings in the heart, *MEOX1* expression was induced by TGFβ and suppressed by JQ1 in fibroblasts from lung, liver and kidney in humans—three other organs that often develop pathological fibrosis in the setting of chronic organ dysfunction (Fig. 4g). Furthermore, *MEOX1* expression was significantly upregulated in heart tissue from patients with cardiomyopathy and in lung tissue from patients with idiopathic pulmonary fibrosis, two human diseases that prominently feature pathological fibrosis[22] (Extended Data Fig. 12c, d).

Conclusion

This study uncovers an essential MEOX1-dependent transcriptional switch that governs cellular plasticity in the fibroblast compartment during the pathogenesis of chronic heart failure and demonstrates that this maladaptive cell state transition is a druggable feature of disease (Fig. 4h). Our work highlights that single-cell-based investigation of cell states in a diseased tissue, coupled with temporally controlled perturbation of transcription signalling, can be used to discover the plasticity of cell states and molecular mechanisms that are critical for the progression and reversal of fibrotic diseases. In contrast to the broad effects of systemic BET inhibition, mechanistic refinement converging on cell-type-specific enhancers in the context of a complex tissue offers the opportunity to develop therapeutic approaches that are tailored to targeted gene regulation in defined cell compartments. These findings may inform new therapeutic strategies for a wide variety of chronic disorders that feature maladaptive remodelling of cell state and tissue architecture.

Online content

Any methods, additional references, Nature Research reporting summaries, source data, extended data, supplementary information, acknowledgements, peer review information; details of author contributions and competing interests; and statements of data and code availability are available at https://doi.org/10.1038/s41586-021-03674-1.

1. Rockey, D. C., Bell, P. D. & Hill, J. A. Fibrosis—a common pathway to organ injury and failure. *N. Engl. J. Med.* **372**, 1138–1149 (2015).
2. Jun, J.-I. & Lau, L. F. Resolution of organ fibrosis. *J. Clin. Invest.* **128**, 97–107 (2018).
3. Anand, P. et al. BET bromodomains mediate transcriptional pause release in heart failure. *Cell* **154**, 569–582 (2013).
4. Spiltoir, J. I. et al. BET acetyl-lysine binding proteins control pathological cardiac hypertrophy. *J. Mol. Cell. Cardiol.* **63**, 175–179 (2013).
5. Duan, Q. et al. BET bromodomain inhibition suppresses innate inflammatory and profibrotic transcriptional networks in heart failure. *Sci. Transl. Med.* **9**, eaah5084 (2017).
6. Stratton, M. S. et al. Dynamic chromatin targeting of BRD4 stimulates cardiac fibroblast activation. *Circ. Res.* **125**, 662–677 (2019).
7. Antolic, A. et al. BET bromodomain proteins regulate transcriptional reprogramming in genetic dilated cardiomyopathy. *JCI Insight* **5**, e138687 (2020).
8. Virani, S. S. et al. Heart disease and stroke statistics—2020 update: a report from the American Heart Association. *Circulation* **141**, e139–e596 (2020).
9. Filippakopoulos, P. et al. Selective inhibition of BET bromodomains. *Nature* **468**, 1067–1073 (2010).
10. Kanisicak, O. et al. Genetic lineage tracing defines myofibroblast origin and function in the injured heart. *Nat. Commun.* **7**, 12260 (2016).
11. Buenrostro, J. D., Wu, B., Chang, H. Y. & Greenleaf, W. J. ATAC-seq: a method for assaying chromatin accessibility genome-wide. *Curr. Protoc. Mol. Biol.* **109**, 21.29.1–21.29.9 (2015).
12. Przytycki, P. F. & Pollard, K. S. CellWalker integrates single-cell and bulk data to resolve regulatory elements across cell types in complex tissues. *Genome Biol.* **22**, 61 (2021).
13. Mahat, D. B. et al. Base-pair-resolution genome-wide mapping of active RNA polymerases using precision nuclear run-on (PRO-seq). *Nat. Protocols* **11**, 1455–1476 (2016).
14. De Santa, F. et al. A large fraction of extragenic RNA pol II transcription sites overlap enhancers. *PLoS Biol.* **8**, e1000384 (2010).
15. Gilbert, L. A. et al. CRISPR-mediated modular RNA-guided regulation of transcription in eukaryotes. *Cell* **154**, 442–451 (2013).
16. Whyte, W. A. et al. Master transcription factors and mediator establish super-enhancers at key cell identity genes. *Cell* **153**, 307–319 (2013).
17. Skuntz, S. et al. Lack of the mesodermal homeodomain protein MEOX1 disrupts sclerotome polarity and leads to a remodeling of the cranio-cervical joints of the axial skeleton. *Dev. Biol.* **332**, 383–395 (2009).
18. Lu, D. et al. Meox1 accelerates myocardial hypertrophic decompensation through Gata4. *Cardiovasc. Res.* **114**, 300–311 (2018).
19. Wei, Z. et al. Molecular mechanism of mesenchyme homeobox 1 in transforming growth factor β1-induced *P311* gene transcription in fibrosis. *Front. Mol. Biosci.* **7**, 59 (2020).
20. Litviňuková, M. et al. Cells of the adult human heart. *Nature* **588**, 466–472 (2020).
21. Domcke, S. et al. A human cell atlas of fetal chromatin accessibility. *Science* **370**, eaba7612 (2020).
22. Sivakumar, P. et al. RNA sequencing of transplant-stage idiopathic pulmonary fibrosis lung reveals unique pathway regulation. *ERJ Open Res.* **5**, 00117-2019 (2019).

Article

a Genes suppressed by JQ1 in TAC model

LV whole tissue bulk RNA-seq (*Duan et al, 2017*) 1,110 84 Bulk RNA-seq from purified CM

22

b Fibroblasts | Myeloid | Endothelial −2 −1 0 1 2 Expression

Top 5 genes per cluster

Gsn, Dcn, Mfap5, Pi16, Gpx3, Lyz2, Wfdc17, C1qa, C1qb, C1qc, Fabp4, Aqp1, Gpihbp1, Ly6c1, 1190002H23Rik, Rgs5, Kcnj8, Vtn, Abcc9, Higd1b, H19, Cpe, Npr3, Tm4sf1, Vwf, Stmn1, Hmgb2, Top2a, 2810417H13Rik, Birc5, Mmrn1, Pard6g, Reln, Fgl2, Ccl21a, Wif1, Dbi, Id4, Dpt, Ccdc80, Prnp, Kcna1, Plp1, Gfra3

Clusters 0 1 2 3 4 5 6 8 7

c Endothelial, Epicardium, Endocardium, Myeloid, Fibroblasts

Dcn — Expression 0 2 4 6

Postn — 0 1 2 3 4 5

Ctgf — 0 1 2 3 4 5

Fabp4 — 0 2 4 6

Lyz2 — 0 2 4 6

d Myeloid — 8 samples 7,986 cells

e Endothelial — 8 samples 10,672 cells

- Sham
- TAC
- TAC JQ1
- TAC JQ1 withdrawn

Extended Data Fig. 1 | Single-cell transcriptional landscape of non-cardiomyocytes in heart failure during intermittent exposure to BET bromodomain inhibition. a, Venn diagram showing overlap of TAC-induced and JQ1-suppressed genes ($\log_2[FC] > 0.5$; adjusted $P < 0.05$; false-discovery rate-adjusted, Benjamini–Hochberg correction) between bulk RNA-seq from undissociated left ventricle tissue[5] and extracted cardiomyocytes. **b**, Heat map showing the top-5 markers per cluster in the scRNA-seq data. Total cells, $n = 35,551$ in 9 clusters. **c**, UMAP plots showing cluster identity of all cells ($n = 35,551$) and expression of *Dcn*, *Postn*, *Ctgf*, *Lyz2* and *Fabp4*. **d, e**, UMAP plot coloured by sample identity of myeloid (**d**, $n = 7,986$) and endothelial (**e**, $n = 10,672$) cells.
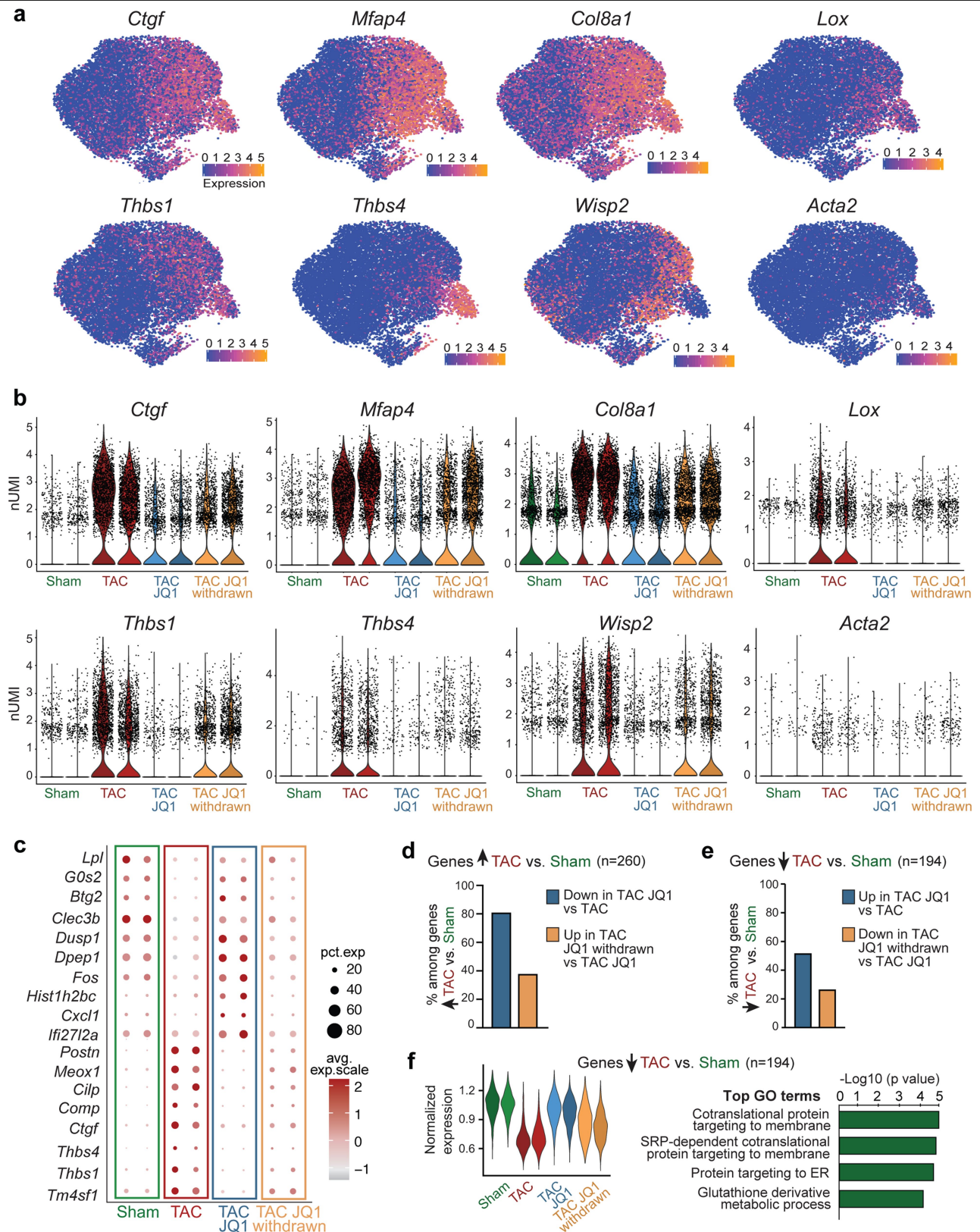
Extended Data Fig. 2 | Reversible effect of JQ1 exposure on the transcriptional signature of baseline and stressed fibroblasts. **a**, Expression of known fibroblast stress-related genes shown as a UMAP feature plots in fibroblasts (total cells, n =13,937). **b**, Expression by sample of known fibroblast stress-related genes shown as violin plots in fibroblasts. y axes, normalized UMI levels. **c**, Dot plots showing expression (avg.exp.scale) and cell percentages (pct.exp) of the top differentially expressed marker genes between samples. **d**, Percentages of the 260 genes upregulated in fibroblasts in TAC versus sham that are significantly downregulated in TAC JQ1 versus TAC (blue bar) and upregulated in TAC JQ1 withdrawn versus TAC JQ1 (yellow bar). **e**, Percentages of the 194 genes significantly downregulated in TAC versus sham that are significantly upregulated in TAC JQ1 versus TAC (blue bar) and downregulated in TAC JQ1 withdrawn versus TAC JQ1 (yellow bar). **f**, Violin plots showing the normalized expression score across fibroblast samples of the 194 genes significantly downregulated in TAC versus sham and associated top GO terms (Fisher's exact test).
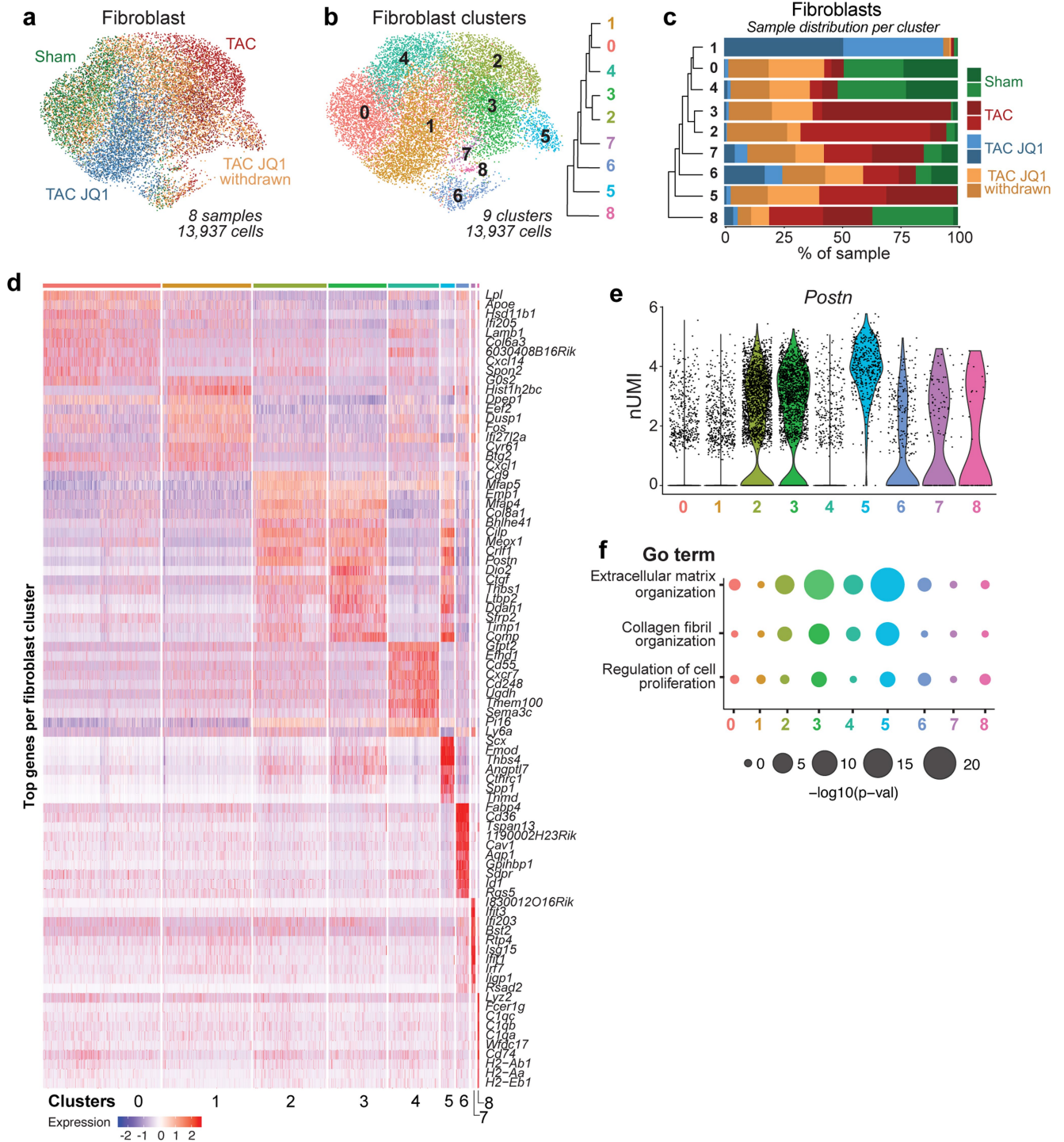
Extended Data Fig. 3 | Fibroblast subclusters associated to stress-related gene programs are depleted in sham and TAC JQ1 cells. a, UMAP plot of fibroblasts coloured by sample identity. $n = 13,937$. **b**, Left, UMAP plot of fibroblast subclusters coloured by cluster identity. Right, a tree diagram showing the cluster relationship. Total cells, $n = 13,937$. **c**, Histograms showing the percentage of each sample in each fibroblast cluster. **d**, Heat map showing the top 10 markers per fibroblast cluster in the scRNA-seq data. Total cells, $n = 13,937$ in 9 clusters. **e**, *Postn* expression in fibroblasts by cluster as violin plots. *y* axes, normalized UMI levels. **f**, Comparative GO term analysis (Fisher's exact test) between fibroblast clusters for fibroblast stress-related biological processes. Top GO terms when analysing the genes driving fibroblast clusters 2, 3 and 5.
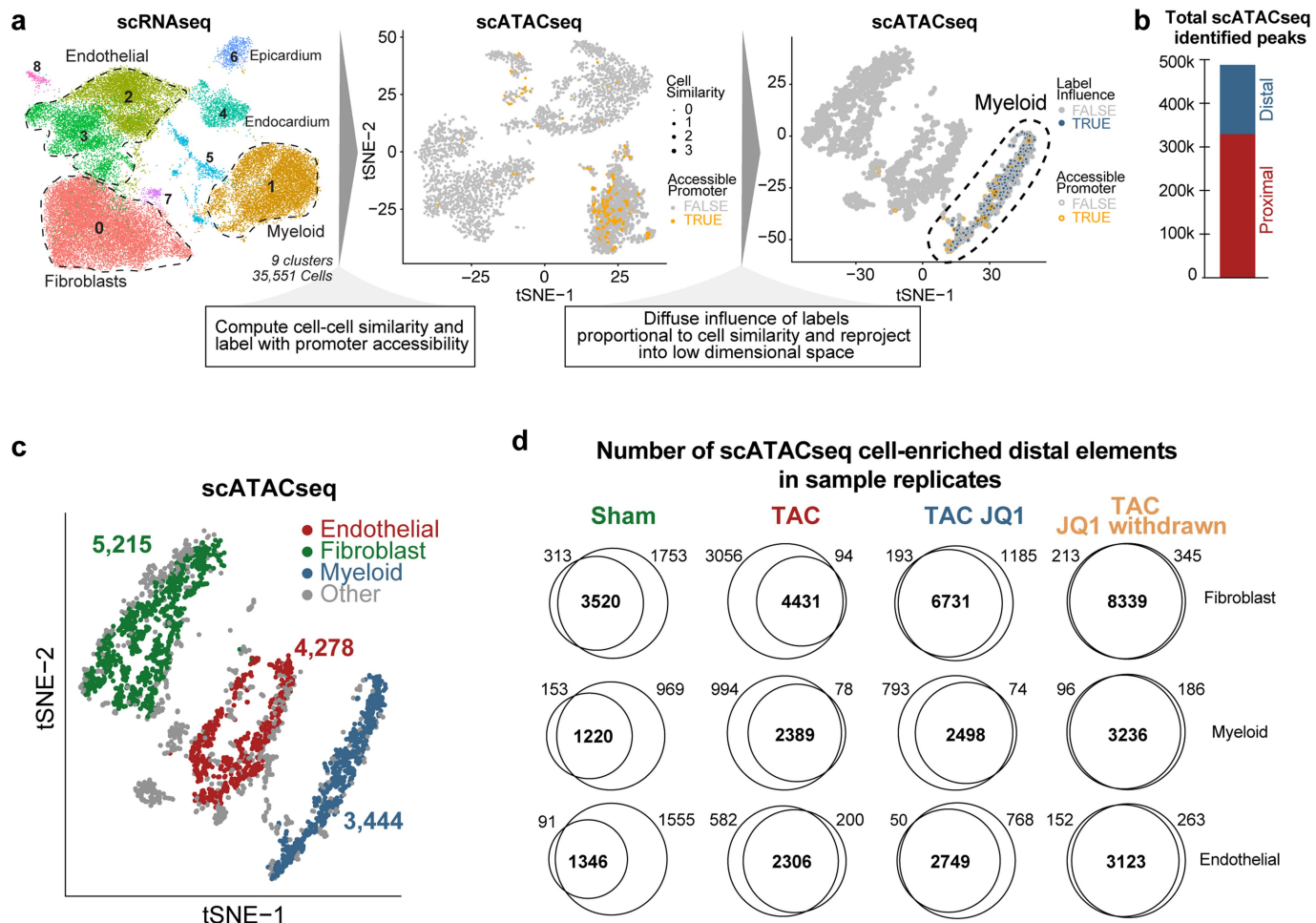
Extended Data Fig. 4 | Defining a catalogue of cell-population-enriched distal elements in fibroblasts, myeloid cells and endothelial cells using scATAC-seq. a, Schematic highlighting the approach to integrate scRNA-seq data with scATAC-seq data[12]. See Supplementary Methods for details. **b**, Total scATAC-seq proximal and distal peaks identified in all cells. **c**, scATAC-seq *t*-SNE plot showing clusters and cell number of fibroblasts, myeloid cells and endothelial cells after integration with scRNA-seq data. **d**, Venn diagrams showing sample replicate convergence of cell-enriched distal elements found with scATAC-seq.

a

Chromatin distal accessibility

Fibroblast: $1.60e^{-23}$, $1.46e^{-18}$ 0.041 $1.01e^{-39}$

Myeloid: 0.015, $7.35e^{-15}$ $1.61e^{-37}$ 0.005

Endothelial: 0.002, $1.07e^{-50}$ $3.43e^{-110}$ $3.60e^{-12}$

Legend: Sham, TAC, TAC JQ1, TAC JQ1 withdrawn

b

Open / Closed

Opening/Closing distal accessible regions
(Heatmap height is normalized on number of regions)

Fibroblast — Sham, TAC, TAC JQ1, TAC JQ1 withdrawn — 4394 regions

Accessibility trend / **Cluster gene ontology** / −Log10 (p-val)

Cluster 2 n=648
- Reg. of heart growth
- ECM organization
- Response to growth factor

Cluster 6 n=495
- Pos. reg. of cell prolif.
- Reg. of cell adhesion
- Reg. of response to stress

Cluster 9 n=1745
- Cardiovacular system dev
- Embryo morphogenesis
- Connective tissue dev

Cluster 11 n=89
- Embryo dev
- Tissue dev
- Embryo pattern spec.

Cluster 12 n=760
- Tube dev
- Skeletal system dev
- Connective tissue dev

Cluster 14 n=350
- Response to wounding
- Reg. of epithelial cell prolif.
- Embryo organ dev

Samples

Myeloid — 1325 regions

Cluster gene ontology / −Log10 (p-val)

Cluster 2 n=176
- Neg. reg. of apoptotic process
- Neg. reg. of cell death
- Reg. of apoptotic process

Endothelial — 1626 regions

Cluster gene ontology / −Log10 (p-val)

Cluster 2 n=50
- Pos. reg. of catalytic activity
- Pos. reg. of molecular function
- reg. of molecular function

c

Fibroblast

	Sham to TAC	TAC to TAC JQ1	TAC JQ1 to TAC JQ1 withdrawn
JUNB			
EGR1			
CEBPB			
JUN			
TCF4			
KLF4			
MEOX1			
NR4A1			
TBX20			
RORA			

Enrichment score TF motif
−1 −0.5 0 0.5 1

Myeloid

	Sham to TAC	TAC to TAC JQ1	TAC JQ1 to TAC JQ1 withdrawn
CEBPB			
JUN			
MAFB			
EGR1			
NFE2L2			
ATF3			
MEF2A			
FOXP1			
FOSL2			
FLI1			

Enrichment score TF motif
−1 −0.5 0 0.5 1

Endothelial

	Sham to TAC	TAC to TAC JQ1	TAC JQ1 to TAC JQ1 withdrawn
JUNB			
JUN			
TCF4			
KLF4			
EGR1			
ETS1			
FLI1			
SOX17			
MEF2A			
MEF2C			

Enrichment score TF motif
−1 −0.5 0 0.5 1

Extended Data Fig. 5 | See next page for caption.

Article

a

+Tam 5 days

Tcf21^{MCM/+}; Rosa26^{Ai6/+}

Langendorff perfusion and isolation of cardiac cells → Sorting of cardiac fibroblasts (ZsGreen1+)

TGFβ ← Unstim ← Fibroblast immortalization (SV40 large T-antigen)

+TGFβ

b

	Postn	*aSMA*	*Ctgf*	*Wisp2*	*Col8a1*
	0.009	8.60e^{-4}	1.40e^{-6}	1.60e^{-7}	7.60e^{-5}

Rel. expression

☐ Unstim ■ TGFβ

c

PROseq
r(pearson)=0.9968

PROseq
r(pearson)=0.9937

d PROseq at distal elements

Unstim TGFβ

2101
1270

LogFC>0.5
p-val<0.05

z-score −1 0 1

e PROseq at protein coding genes

Unstim TGFβ

632
709

LogFC>0.5
p-val<0.05

z-score −1 0 1

Top GO terms	p-val	Gene
ECM organization	5.6e^{-8}	*Postn* *Pdgfa*
Pos. regulation of cell motility	7.6e^{-6}	*Pdgfb* *Pdgfc* *Igf1*
Pos. regulation of cell migration	2.5e^{-4}	*Lef1* *Sema7a*

Top GO terms	p-val	Gene
ECM organization	5.5e^{-4}	*Col6a1* *Itga8*
Neg. regulation of response to stimulus	3.7e^{-3}	*Icam1* *Ror1* *Fgfr2*
Neg. regulation of cell adhesion	3.7e^{-3}	*Plxna2* *Dscam*

f

Metagene analysis at genes
↑TGFβ vs. Unstim

PROseq tag+ density
n=632 genes

Metagene analysis at genes
↓TGFβ vs. Unstim

PROseq tag+ density
n=709 genes

g

Metagene analysis at genes identified in scRNAseq
↑TAC vs. Sham

PROseq tag+ density
n=260 genes

Metagene analysis at genes identified in scRNAseq
↓TAC vs. Sham

PROseq tag+ density
n=194 genes

h

Co-Accessibility (CoAc) of *Postn* Peak 10/11 with gene promoters within 1Mb of the peak

● = *Postn* promoter

Change in Fibroblast CoAc

Sham to TAC | TAC to TAC JQ1 | TAC JQ1 to TAC JQ1 withdrawn

i

☐ Unstim ■ TGFβ

Postn

2.60e^{-4}

Rel. expression

CRISPRi Control line

j *Postn*

Peak8 eRNA

5.40e^{-5}
ns

Rel. expression

CRISPRi Control line | CRISPRi *Postn* Peak8

Peak10/11 eRNA

5.70e^{-11}
2.60e^{-6}

CRISPRi Control line | CRISPRi *Postn* Peak11

Peak19 eRNA

0.001
ns

CRISPRi Control line | CRISPRi *Postn* Peak19

☐ Unstim ■ TGFβ

k H3K9me3 at *Postn* locus

Unstim

2.20e^{-12}

2.20e^{-8}

ns

% of INPUT

Peak11 | Peak10 | Promoter

☐ CRISPRi Control line
■ CRISPRi *Postn* Peak11

TGFβ

5.50e^{-5}

0.043

ns

% of INPUT

Peak11 | Peak10 | Promoter

Extended Data Fig. 6 | See next page for caption.

Article

**Extended Data Fig. 6 | Nascent transcription in TGFβ-treated cells identifies stress-responsive distal and gene elements. a**, Schematic of the isolation and immortalization of mouse adult cardiac fibroblasts. **b**, Expression by qPCR of canonical markers of activated fibroblasts in unstimulated (Unstim) and TGFβ-treated cells. Unpaired, two-tailed Student's *t*-test. **c**, Pearson correlation of the two independent biological replicates of PRO-seq in unstimulated and TGFβ-treated cells. **d**,**e**, Heat map of PRO-seq coverage of differentially transcribed distal regions (**d**) and protein-coding genes (**e**, right) between unstimulated and TGFβ-treated fibroblasts. Wald test with Benjamini–Hochberg correction. Signal for replicates 1 and 2 is shown. **e**, Right, top associated GO terms (Fisher's exact test). **f**, PRO-seq tag density (±5 kb gene body) in unstimulated and TGFβ-treated cells in the genes differentially transcribed in unstimulated versus TGFβ-treated. Top, genes upregulated after TGFβ treatment. Bottom, genes downregulated after TGFβ treatment. **g**, PRO-seq tag density (±5 kb gene body) in unstimulated and TGFβ-treated cells in the set of genes upregulated (left, $n = 260$) or downregulated (right, $n = 194$) in TAC versus sham in fibroblasts in vivo. **h**, Co-accessibility (CoAc) change in fibroblasts of *Postn* peak 10/11 element with the promoters of genes within 1 Mb

of the peak. Change in co-accessibility with the *Postn* promoter is highlighted in red. $n = 27$ genes within 1 Mb. Box plots show the 25th, 50th and 75th percentiles, with whiskers extending to the furthest value no further than 1.5× the interquartile range. **i**, *Postn* expression measured by qPCR in unstimulated and TGFβ-treated in the CRISPRi control line. Unpaired, two-tailed *t*-test. **j**, *Postn* peak 8, 10/11 and 19 eRNA expression measured by qPCR in unstimulated and TGFβ-treated fibroblasts in a CRISPRi control line and lines targeting peak 8, peak 10/11 or peak 19. Values are normalized to the CRISPRi control line in the unstimulated condition. One-way ANOVA followed by Sidak's correction, statistical significance is shown between the unstimulated samples and TGFβ-treated samples. **k**, ChIP–qPCR data showing enrichment over chromatin input of H3K9me3 in control and *Postn* peak 10/11 CRISPRi lines in the unstimulated (left) and TGFβ-treated (right) condition. Regions amplifying peak 10, peak 11 and *Postn* promoters are shown. One-way ANOVA followed by Sidak's correction, statistical significance is shown between control and *Postn* peak 10/11 CRISPRi lines. **b**, **i**–**k**, Numbers above histograms show significant *P* values. Data are mean ± s.e.m.
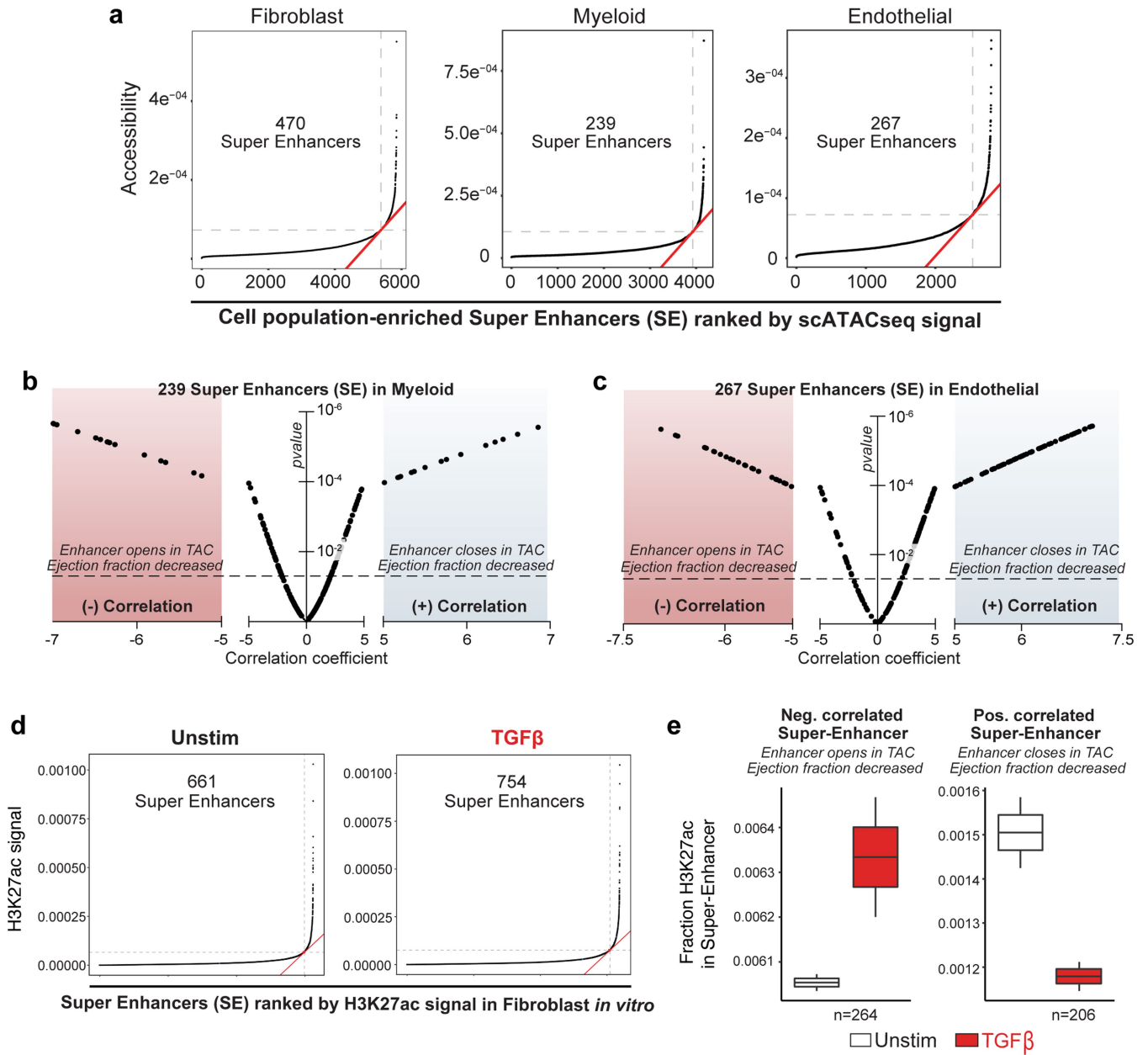
Extended Data Fig. 7 | Characterization of a catalogue of super-enhancers in fibroblasts, myeloid cells and endothelial cells. a, Distribution of accessibility in fibroblasts, myeloid cells and endothelial cells in the TAC state identifies a class of distal regions (super-enhancers (SE)) for which the accessibility falls over the inflection point of the curve. **b**, **c**, Volcano plots showing correlation coefficients and corresponding *P* values (refer to the analysis depicted in Fig. 2e) of 239 super-enhancers in myeloid (**b**) and 267 super-enhancers in endothelial (**c**) cells. **d**, Distribution of H3K27ac in unstimulated and TGFβ-treated fibroblasts identifies a class of distal regions (super-enhancers) for which the accessibility falls over the inflection point of the curve. **e**, Fraction of H3K27ac in unstimulated and TGFβ-treated fibroblasts for the enhancers identified in vivo having a negative (left, *n* = 264) or positive (right, *n* = 206) correlation with heart function (based on analysis depicted in Fig. 2e). Box plots show the 25th, 50th and 75th percentiles, with whiskers extending to the furthest value no further than 1.5× the interquartile range.
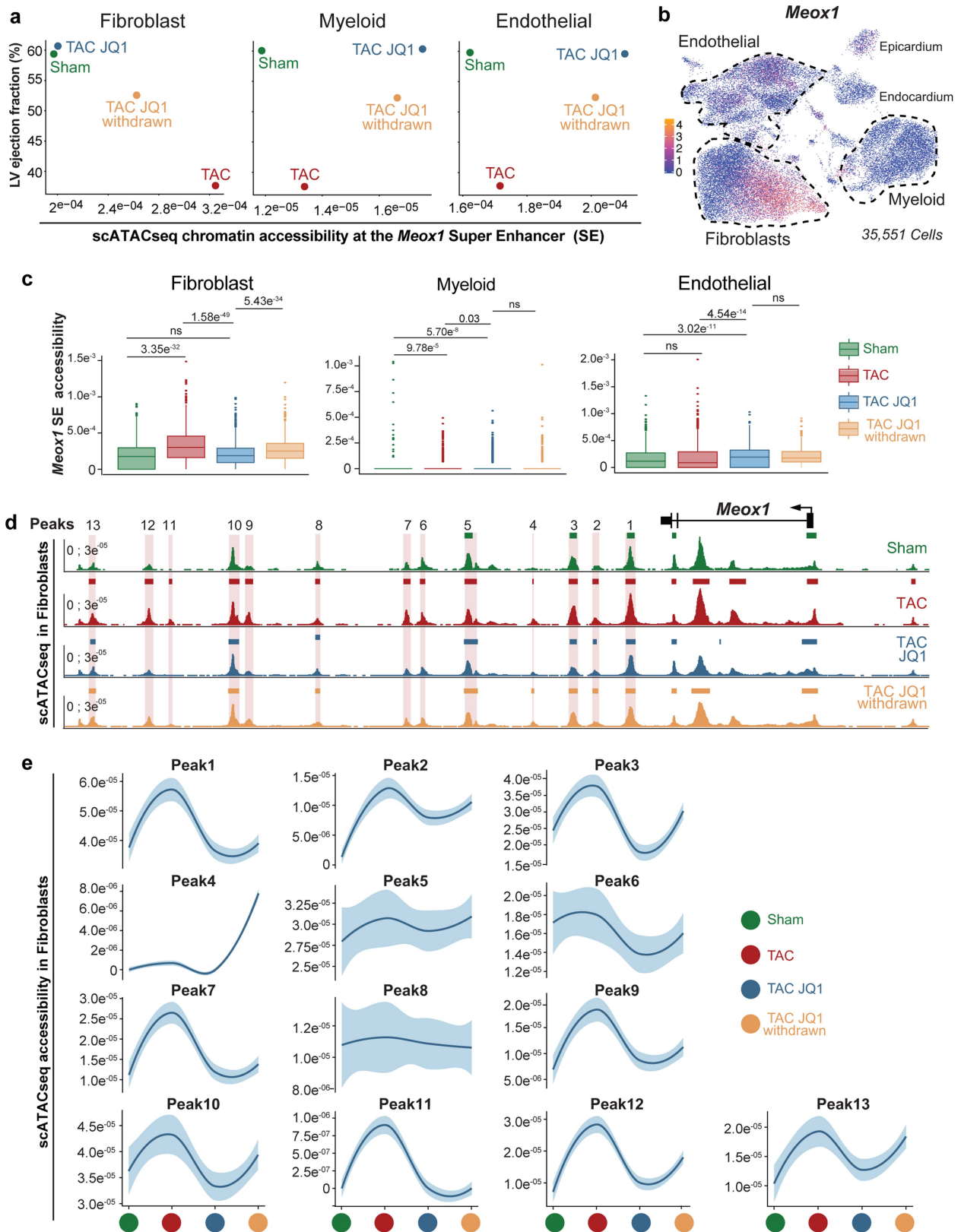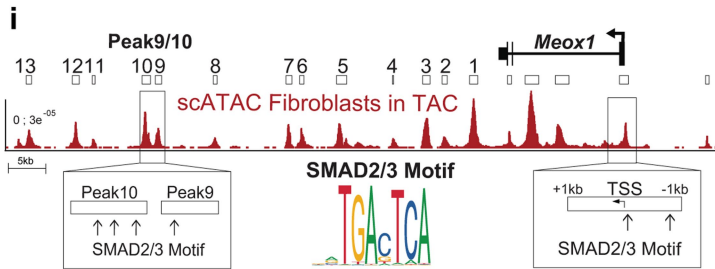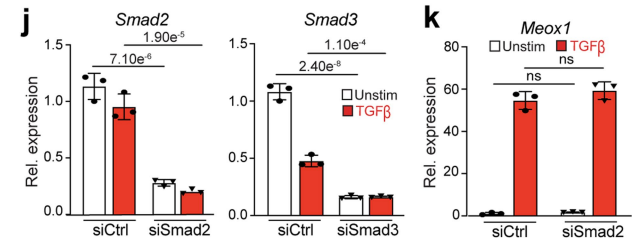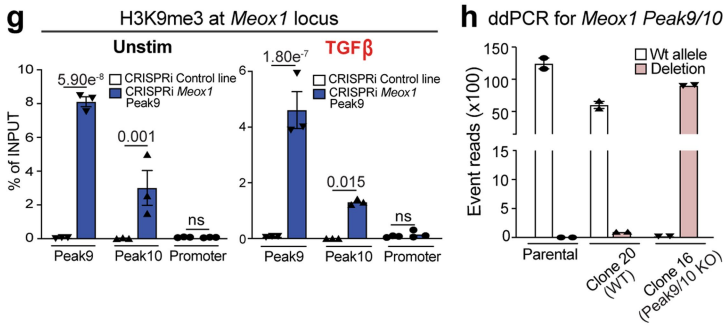
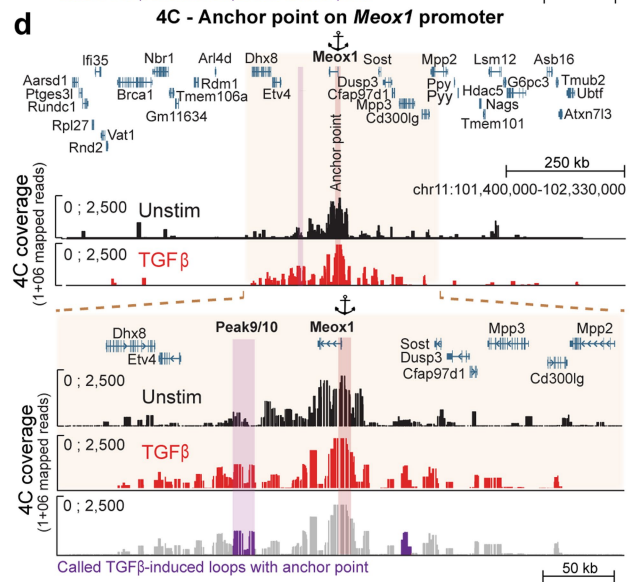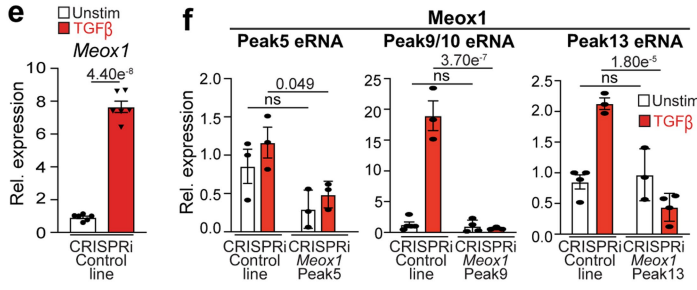**Extended Data Fig. 8** | See next page for caption.

Extended Data Fig. 8 | Dynamic changes in chromatin accessibility at the *Meox1* super-enhancer. a, Comparison of left ventricle ejection fraction with chromatin accessibility at the *Meox1* super-enhancer in fibroblasts, myeloid cells and endothelial cells. **b**, UMAP plot of *Meox1* expression in all non-cardiomyocytes ($n = 35,551$). **c**, Chromatin accessibility at the *Meox1* super-enhancer between samples in fibroblasts, myeloid cells and endothelial cells. Box plots show the 25th, 50th and 75th percentiles, with whiskers extending to the furthest value no further than 1.5× the interquartile range. Sample sizes (from left to right for each cell type): fibroblasts ($n = 676, 979, 1,906, 1,654$), myeloid cells ($n = 631, 1,080, 1,021, 712$), endothelial cells ($n = 731, 1,666, 1,030, 851$). Numbers above box plots show significant *P* values, statistical significance (two-sided Wilcoxon rank-sum test) is shown for: sham versus TAC, sham versus TAC JQ1, TAC versus TAC JQ1 and TAC JQ1 versus TAC JQ1 withdrawn. **d**, scATAC-seq average signal across cells in fibroblast samples at the *Meox1* super-enhancer identifies multiple dynamic peaks in heart failure with pulsatile exposure to BET inhibition. **e**, Chromatin accessibility trend between samples (mean and 95% confidence interval) in all identified *Meox1* super-enhancer peaks.
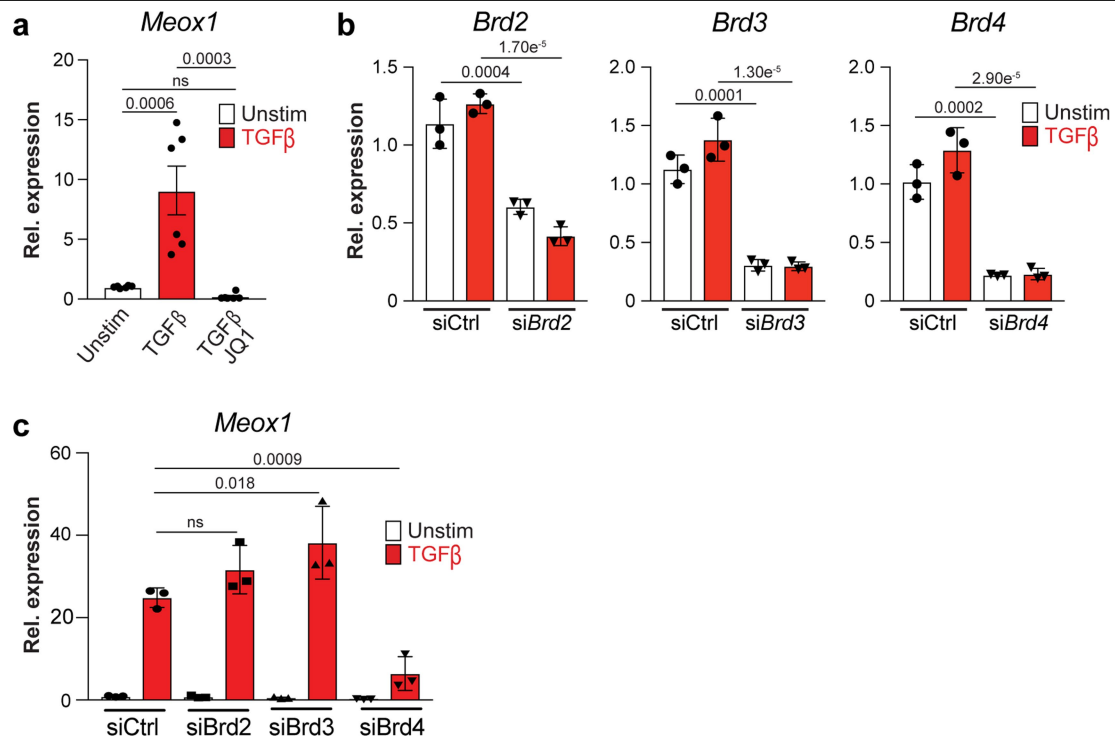
Extended Data Fig. 9 | *Brd4*-dependent regulation of *Meox1* expression.
a, *Meox1* expression measured by qPCR in unstimulated and TGFβ-treated fibroblasts, treated with or without JQ1. **b**, Expression measured by qPCR of individual BET genes in unstimulated or TGFβ-treated fibroblasts treated with siRNA targeting control (siCtrl), *Brd2* (si*Brd2*), *Brd3* (si*Brd3*) or *Brd4* (si*Brd4*). Statistical significance is shown between unstimulated samples and TGFβ-treated samples. **c**, *Meox1* expression measured by qPCR in unstimulated or TGFβ-treated fibroblasts treated with siRNA targeting control, *Brd2*, *Brd3* or *Brd4*. Statistical significance is shown between the TGFβ and control siRNA sample and the other TGFβ-treated samples. **a**–**c**, All analysed samples were biological replicates. Numbers above graphs show significant *P* values (one-way ANOVA followed by Tukey post hoc test). Data are mean ± s.e.m.

a Nascent transcription (PROseq) at all scATACseq peaks in Fibroblasts

● *Meox1* Peak9 ● *Meox1* Peak10

b Co-Accessibility (CoAc) of *Meox1* Peak 9/10 with gene promoters within 1Mb of the peak

● = *Meox1* promoter

c 4C - Anchor point on *Meox1* Peak9/10

d 4C - Anchor point on *Meox1* promoter

e *Meox1*

f Meox1

Peak5 eRNA   Peak9/10 eRNA   Peak13 eRNA

g H3K9me3 at *Meox1* locus

h ddPCR for *Meox1 Peak9/10*

i Peak9/10   *Meox1*

scATAC Fibroblasts in TAC

SMAD2/3 Motif

j *Smad2*   *Smad3*

k *Meox1*

Extended Data Fig. 10 | See next page for caption.

Extended Data Fig. 10 | The peak 9/10 *Meox1* enhancer is strongly transcribed after TGFβ stimulation. a, Volcano plot showing the $\log_2$[FC] of the PRO-seq signal of all identified distal scATAC-seq peaks in fibroblasts (n = 9,211) between unstimulated and TGFβ-treated fibroblasts. *Meox1* peaks 9 (red) and 10 (orange) are highlighted. **b**, Co-accessibility change in fibroblasts of *Meox1* peak 9/10 element with the promoters of genes within 1 Mb of the peak. Change in co-accessibility with the *Meox1* promoter is highlighted in red. n = 115 genes within 1 Mb. Box plots show the 25th, 50th and 75th percentiles, with whiskers extending to the furthest value no further than 1.5× the interquartile range. **c**, **d**, Chromosome conformation capture (4C) using the *Meox1* peak 9/10 region (**c**) or *Meox1* promoter (**d**) as anchor point. 4C coverage in unstimulated and TGFβ-treated fibroblasts are shown in a 922-kb (top) and 328-kb (bottom) genomic regions. The last track represents the called TGFβ-induced loops with the anchor point (coloured in purple). **e**, *Meox1* expression measured by qPCR in unstimulated and TGFβ-treated fibroblasts in the CRISPRi control line. Unpaired, two-tailed *t*-test. **f**, *Meox1* peak 5, 9/10 and 13 eRNA expression measured by qPCR in unstimulated and TGFβ-treated fibroblasts in a CRISPRi control line and lines targeting peak 5, peak 9/10 or peak 13. Values are normalized to the CRISPRi control line in the unstimulated condition. One-way ANOVA followed by Sidak's correction, statistical significance is shown between unstimulated samples and TGFβ-treated samples. **g**, ChIP–qPCR data showing enrichment over chromatin input of H3K9me3 in control and *Meox1* peak 9/10 CRISPRi lines in the unstimulated (left) and TGFβ-treated (right) conditions. Regions amplifying peak 9, peak 10 and *Meox1* promoters are shown. One-way ANOVA followed by Sidak's correction, statistical significance is shown between CRISPRi control and targeted lines. **h**, Droplet digital (dd)PCR amplifying a wild-type or mutated region of *Meox1* peak 9/10 DNA. Parental fibroblast cell line, wild type (clone 20, isogenic control exposed to CRISPR Cas9 and gRNAs) and peak 9/10 knockout (KO) (clone 16) cell lines are shown. **i**, Schematic showing the *Meox1* locus with the scATAC-seq average signal across fibroblasts in TAC. SMAD2/3 motifs (Jaspar, MA1622.1) in the peak 9/10 region and in the *Meox1* promoter (±1 kb from the transcription start site (TSS)) are highlighted. **j**, Expression measured by qPCR of *Smad2* (left) and *Smad3* (right) in unstimulated or TGFβ-treated fibroblasts with siRNA targeting control and *Smad2* (left) or *Smad3* (right). One-way ANOVA followed by Tukey post hoc test. **k**, *Meox1* expression measured by qPCR in unstimulated or TGFβ-treated fibroblasts with siRNA targeting either control or *Smad2*. One-way ANOVA followed by Tukey post hoc test. **e**–**g**, **j**, **k**, Numbers above histograms show significant *P* values. Data are mean ± s.e.m.
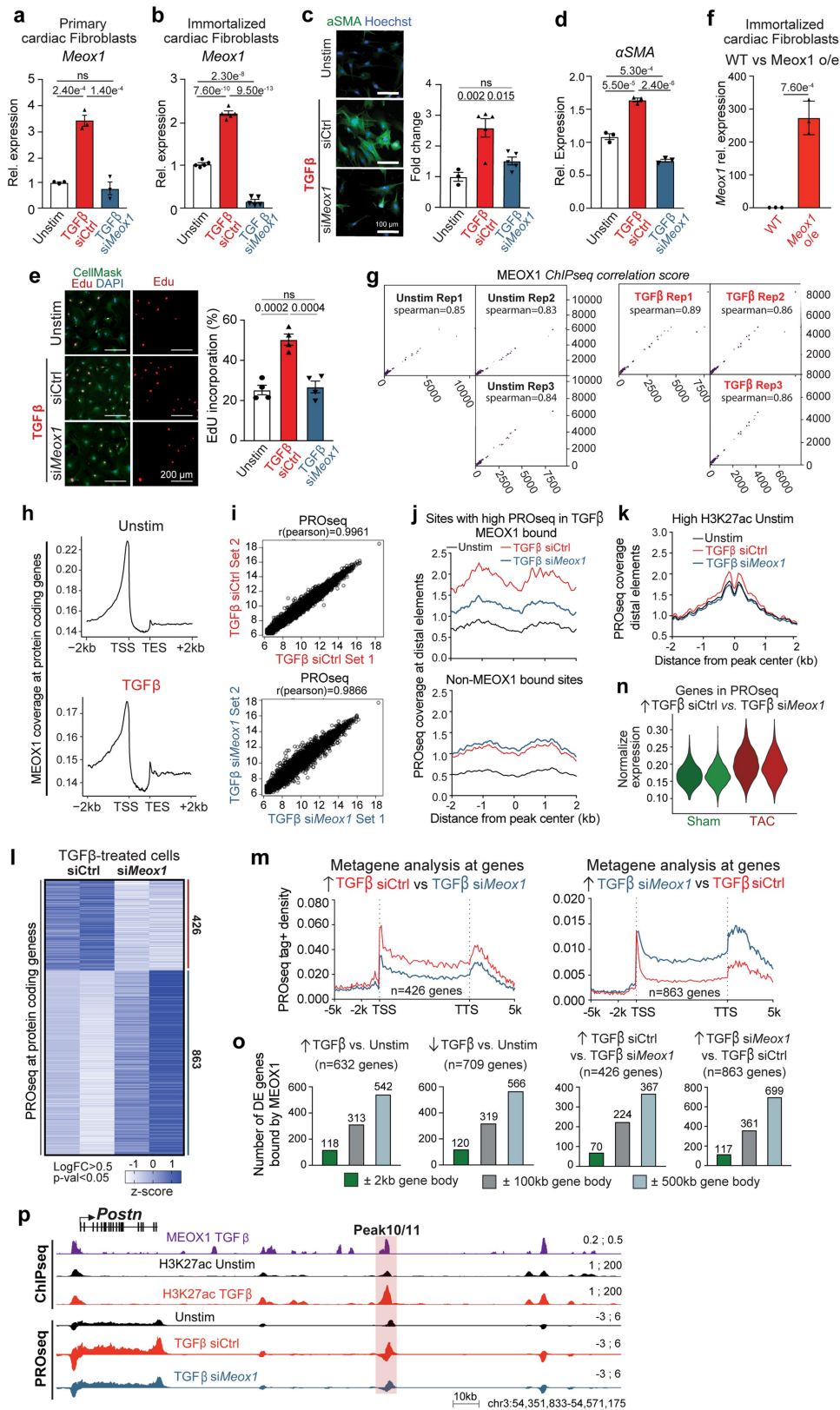
Extended Data Fig. 11 | See next page for caption.

Article

Extended Data Fig. 11 | MEOX1 is a regulator of fibroblast activation.
a, **b**, *Meox1* expression measured by qPCR in mouse primary cardiac fibroblasts
(**a**) and immortalized cardiac fibroblasts (**b**) in the unstimulated condition, or
after treatment with TGFβ and control siRNA or TGFβ and *Meox1* siRNA. One-
way ANOVA followed by Tukey post hoc test. **c**, Left, immunofluorescence
staining of αSMA in unstimulated and TGFβ-treated cells treated with a control
or a *Meox1*-targeting siRNA. Nuclei are marked by Hoechst. Scale bars, 100 μm.
Right, quantification of αSMA staining (two independent experiments). The
fold change in intensity is normalized to the cell number. One-way ANOVA
followed by Tukey post hoc test. **d**, Expression of *Acta2* (which encodes αSMA)
measured by qPCR in the unstimulated condition, or after treatment with TGFβ
and control siRNA or TGFβ and *Meox1* siRNA. One-way ANOVA followed by
Tukey post hoc test. **e**, Left, representative images of EdU incorporation in the
unstimulated condition, or after treatment with TGFβ and control siRNA or
TGFβ and *Meox1* siRNA. DAPI (blue), EdU (red) and CellMask (green). Scale bars,
200 μm. Right, quantification (two independent experiments). One-way
ANOVA followed by Tukey post hoc test. **f**, *Meox1* expression measured by qPCR
in wild-type and *Meox1* overexpression (o/e) mouse immortalized cardiac
fibroblasts. Unpaired, two-tailed *t*-test. **g**, Pearson correlation of the three
replicates of MEOX1 anti-haemagglutinin (HA) ChIP–seq in unstimulated and
TGFβ-treated cells. **h**, MEOX1 anti-HA ChIP–seq coverage in all protein-coding
genes (±2 kb gene body) in unstimulated and TGFβ-treated fibroblasts.
i, Pearson correlation of the two independent biological replicates of PRO-seq
for TGFβ and control siRNA or TGFβ and *Meox1* siRNA treatments. **j**, PRO-seq
coverage in the unstimulated condition, and after treatment with TGFβ and
control siRNA or TGFβ and *Meox1* siRNA at the distal elements defined as more

transcribed in TGFβ versus unstimulated (2,101 sites) (see Fig. 2a) that are
either bound by MEOX1 (496 regions, top) or not (1,605 regions, bottom).
k, PRO-seq coverage in the unstimulated condition, or after treatment with
TGFβ and control siRNA or TGFβ and *Meox1* siRNA at the distal elements with
high H3K27ac enrichment in the unstimulated condition bound by MEOX1
(379 regions). **l**, PRO-seq coverage of differentially transcribed genes (Wald
test followed by Benjamini–Hochberg correction) in TGFβ-treated fibroblasts
with control or *Meox1* siRNA. Signal for replicates 1 and 2 is shown. **m**, PRO-seq
tag density (±5 kb gene body) after treatment with TGFβ and control siRNA or
TGFβ and *Meox1* siRNA in genes upregulated in TGFβ and control siRNA versus
TGFβ and *Meox1* siRNA (left); and genes upregulated in TGFβ and *Meox1* siRNA
versus TGFβ and control siRNA (right). **n**, Violin plot showing the normalized
expression scores of genes upregulated in TGFβ and control siRNA versus TGFβ
and *Meox1* siRNA in PRO-seq that were captured in the scRNA-seq data.
Expression of sham and TAC fibroblast samples is shown. **o**, Number of MEOX1-
bound genes in MEOX1 ChIP–seq (in TGFβ-treated cells) in ±2 kb gene body,
±100 kb gene body or ±500 kb gene body in genes differentially transcribed in
PRO-seq: upregulated in TGFβ versus unstimulated (left); downregulated in
TGFβ versus unstimulated (centre left); upregulated in TGFβ and control siRNA
versus TGFβ and *Meox1* siRNA (centre right); upregulated in TGFβ and *Meox1*
siRNA versus TGFβ and control siRNA (right). **p**, Coverage of MEOX1 ChIP
(TGFβ-treated cells), H3K27ac ChIP–seq (unstimulated and TGFβ-treated cells)
and PRO-seq (unstimulated condition, or treatment with TGFβ and control
siRNA or TGFβ and *Meox1* siRNA) at the *Postn* locus. The *Postn* peak 10/11 region
is highlighted in red. **a**–**f**, Numbers above graphs show significant *P* values.
Data are means ± s.e.m.

Human adult cardiac FBs

a

POSTN

MEOX1

b

Human fetal heart FB

c

d
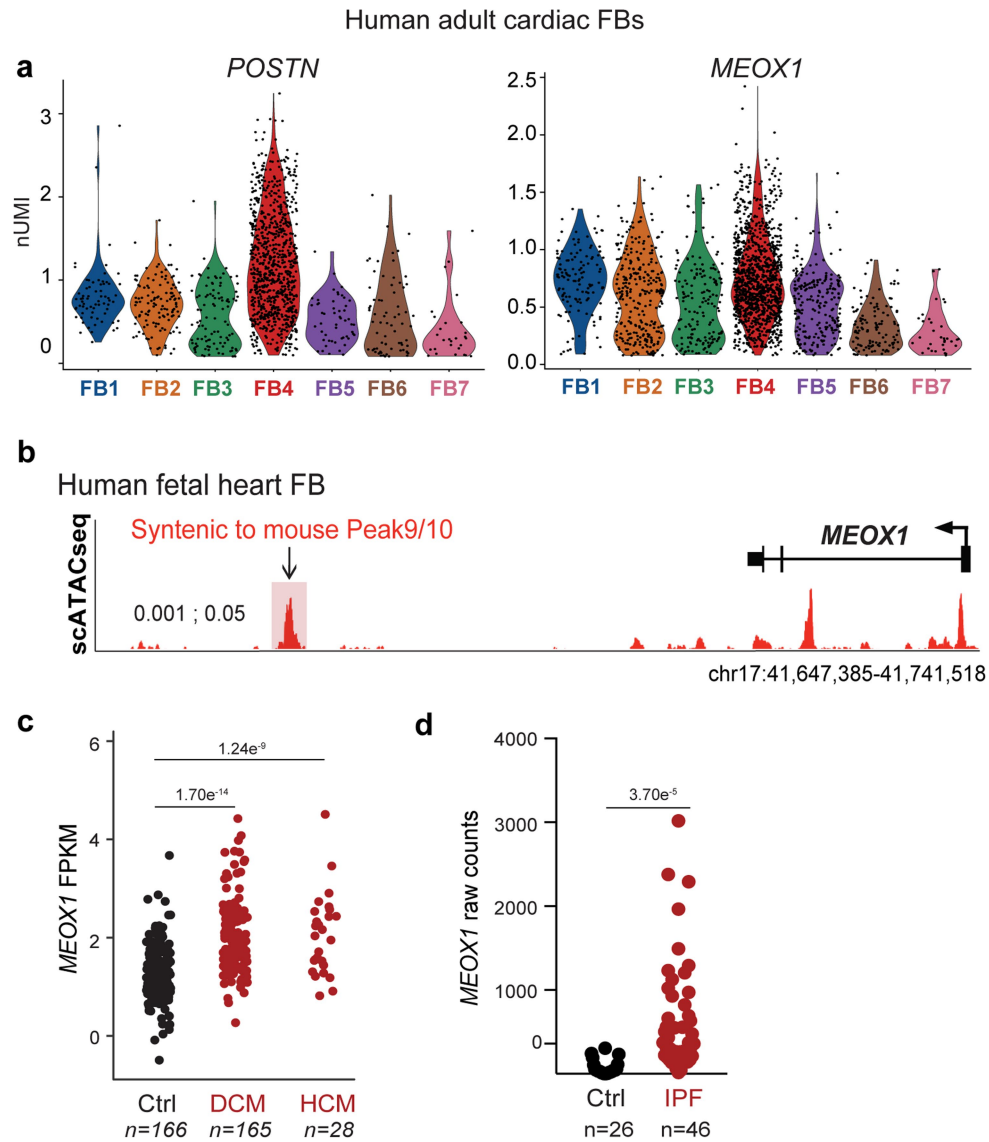
Extended Data Fig. 12 | *MEOX1* is expressed in human activated fibroblasts.
a, *POSTN* (left) and *MEOX1* (right) expression in human adult fibroblast clusters.
y axes, normalized UMI levels[20]. **b**, Track showing scATAC-seq average signal
across fibroblasts in the human fetal heart[21] in the *MEOX1* locus. The syntenic
region of peak 9/10 is highlighted in red. **c**, Bulk RNA-seq data of human *MEOX1*
expression (fragments per kilobase of transcript per million mapped reads,
FPKM) in heart tissue in control individuals (Ctrl) and individuals with dilated
cardiomyopathy (DCM) or hypertrophic cardiomyopathy (HCM) (GSE141910).
Unpaired, two-tailed *t*-test with Benjamini–Hochberg correction. **d**, Bulk
RNA-seq data of human *MEOX1* expression (raw counts) in lung tissue between
control individuals and individuals with idiopathic pulmonary fibrosis (IPF)
(GSE134692)[22]. Unpaired, two-tailed *t*-test. **c**, **d**, Numbers above the graphs
show significant *P* values.

Corresponding author(s): Saptarsi Haldar
Deepak Srivastava

Last updated by author(s): Apr 15, 2021

Reporting Summary

Nature Research wishes to improve the reproducibility of the work that we publish. This form provides structure for consistency and transparency in reporting. For further information on Nature Research policies, see our Editorial Policies and the Editorial Policy Checklist.

Statistics

For all statistical analyses, confirm that the following items are present in the figure legend, table legend, main text, or Methods section.

n/a	Confirmed	
☐	☒	The exact sample size (*n*) for each experimental group/condition, given as a discrete number and unit of measurement
☒	☐	A statement on whether measurements were taken from distinct samples or whether the same sample was measured repeatedly
☐	☒	The statistical test(s) used AND whether they are one- or two-sided *Only common tests should be described solely by name; describe more complex techniques in the Methods section.*
☐	☒	A description of all covariates tested
☐	☒	A description of any assumptions or corrections, such as tests of normality and adjustment for multiple comparisons
☐	☒	A full description of the statistical parameters including central tendency (e.g. means) or other basic estimates (e.g. regression coefficient) AND variation (e.g. standard deviation) or associated estimates of uncertainty (e.g. confidence intervals)
☐	☒	For null hypothesis testing, the test statistic (e.g. *F*, *t*, *r*) with confidence intervals, effect sizes, degrees of freedom and *P* value noted *Give P values as exact values whenever suitable.*
☒	☐	For Bayesian analysis, information on the choice of priors and Markov chain Monte Carlo settings
☒	☐	For hierarchical and complex designs, identification of the appropriate level for tests and full reporting of outcomes
☐	☒	Estimates of effect sizes (e.g. Cohen's *d*, Pearson's *r*), indicating how they were calculated

Our web collection on statistics for biologists contains articles on many of the points above.

Software and code

Policy information about availability of computer code

Data collection	All sequencing were performed using the NextSeq 500 (Illumina, software 4.0.2) and NovaSeq (Illumina, software v1.5).
Data analysis	Cellranger (v2.2.0), R (3.5.1), Seurat (v2.3.4), ImageJ (2.0.0), GraphPad Prism 8, Homer (4.11.1).

For manuscripts utilizing custom algorithms or software that are central to the research but not yet described in published literature, software must be made available to editors and reviewers. We strongly encourage code deposition in a community repository (e.g. GitHub). See the Nature Research guidelines for submitting code & software for further information.

Data

Policy information about availability of data

All manuscripts must include a data availability statement. This statement should provide the following information, where applicable:
- Accession codes, unique identifiers, or web links for publicly available datasets
- A list of figures that have associated raw data
- A description of any restrictions on data availability

All sequencing data have been deposited in NCBI's Gene Expression Omnibus and are accessible through GEO series accession number GSE155882. All processed data have also been included in the GSE155882 (single-cell expression matrices and bigwig files). Other processes data (gene lists and bed files) are provided in the Supplementary Tables.

Public database used: reference genome (mm10).

Field-specific reporting

Please select the one below that is the best fit for your research. If you are not sure, read the appropriate sections before making your selection.

☒ Life sciences ☐ Behavioural & social sciences ☐ Ecological, evolutionary & environmental sciences

For a reference copy of the document with all sections, see nature.com/documents/nr-reporting-summary-flat.pdf

Life sciences study design

All studies must disclose on these points even when the disclosure is negative.

Sample size	No statistical method was used to predetermine sample size. For the in vivo experiments, we used the following number of animals: Sham (n=4), TAC (n=6), TAC JQ1 (n=10), TAC JQ1 withdrawn (n=14). For tissue fibrosis quantification, we used the following number of animals: TAC JQ1 (n=4), TAC JQ1 withdrawn (n=8). For single cell RNA/ATACseq experiments, we loaded 12,000 non-cardiomyocyte cells from the adult mouse heart. We used 2 replicates each conditions for PROseq, 3 replicates per condition for MEOX1-HA ChIPseq, and 2 replicates each condition for H3K27ac ChIPseq. For gene expression analysis by qPCR, the number of samples is indicated as data points on the figures (at least 3 replicates for each conditions).
Data exclusions	No data was excluded from the analysis.
Replication	We performed all experiments in biological replicates and could observe agreement between the replicates. All experiments were performed at least twice independently and material was collected and processed independently and by different researchers. The exact number of replicates, the exact p-value and the statistical test used to obtain it are indicated in the figures and legends.
Randomization	Cellular experiments were done in multi-well plates with randomized choices of the wells for each treatment. For animal experiments, animals were randomized before treatment.
Blinding	All surgeries and echocardiography imaging analyses were blinded with regard to treatment, and animals were decoded only after all data were analyzed. For quantification of picrosirius red staining, aSMA staining and EdU incorporation, a blinded approach was used, samples were labeled with an alphanumeric code and the different conditions were decoded only after the data analysis. Quantification of gene expression by qPCR were performed by applying the same parameters in an unbiased way.

Reporting for specific materials, systems and methods

We require information from authors about some types of materials, experimental systems and methods used in many studies. Here, indicate whether each material, system or method listed is relevant to your study. If you are not sure if a list item applies to your research, read the appropriate section before selecting a response.

Materials & experimental systems

n/a	Involved in the study
☐	☒ Antibodies
☐	☒ Eukaryotic cell lines
☒	☐ Palaeontology and archaeology
☐	☒ Animals and other organisms
☒	☐ Human research participants
☒	☐ Clinical data
☒	☐ Dual use research of concern

Methods

n/a	Involved in the study
☐	☒ ChIP-seq
☒	☐ Flow cytometry
☒	☐ MRI-based neuroimaging

Antibodies

Antibodies used	Anti-HA antibody (Abcam #9110) Anti-H3K27ac (Abcam #ab4729) Picro Sirius Red stained (Abcam #ab150681) aSMA (DAKO # M0851) Donkey anti-mouse IgG 555 antibody (Invitrogen, #A32773) Hoechst (Thermo Scientific, #33342) Each quantity of antibody is specified in the Method sections.
Validation	For the anti-HA used for MEOX1-HA ChIPseq, we validated the anti-HA antibody using positive (pHR lentiviral Meox1-HA overexpression) and negative (overexpression of pHR with no Meox1-HA cassette) and performing Western Blot and IHC. Anti-HA antibody (Abcam #9110), validated by the company, has been referenced in 764 publications.

Anti-H3K27ac (Abcam #ab4729), validated by the company, has been referenced in 1229 publications.
Picro Sirius Red stained (Abcam #ab150681), validated by the company, has been referenced in 92 publications.
aSMA (DAKO # M0851), validated by the company, has been referenced in 1122 publications.
Donkey anti-mouse IgG 555 antibody (Invitrogen, #A-32773), validated by the company, has been referenced in 91 publications.
Hoechst (Thermo Scientific, #33342), validated by the company, has been referenced in 651 publications.

Eukaryotic cell lines

Policy information about cell lines

Cell line source(s)	HEK293 (ATCC); immortalized cardiac fibroblasts (made in house), human lung fibroblasts (ATCC, #CRL-4058), human liver fibroblasts (CELL APPLICATIONS INC, #712-05f); human kidney fibroblasts (Cell Biologics, # H-6016).
Authentication	Cells lines were acquired from ATCC. For the generation of our immortalized cardiac fibroblasts line, we sorted ZsGreen positive cells from a Tcf21MCM/+;Rosa26 Ai6/+ adult mouse (all details reported in the Method section). We have authenticated the cell line performing karyotyping and PCR using species-specific primers.
Mycoplasma contamination	All cell lines tested negative for mycoplasma contamination regularly every 2 weeks
Commonly misidentified lines (See ICLAC register)	No commonly misidentified cell lines were used in the study.

Animals and other organisms

Policy information about studies involving animals; ARRIVE guidelines recommended for reporting animal research

Laboratory animals	For the JQ1-related experiments: C57Bl/6J (The Jackson Laboratory, Stock No: 000664) - Males at the age ranging 10-18 weeks
Wild animals	This study did not use wild animals
Field-collected samples	The study did not involve field-collected samples
Ethics oversight	All protocols concerning animal use were approved by the Institutional Animal Care and Use Committees at the University of California San Francisco and conducted in strict accordance with the National Institutes of Health Guide for the Care and Use of Laboratory Animals.

Note that full information on the approval of the study protocol must also be provided in the manuscript.

ChIP-seq

Data deposition

☒ Confirm that both raw and final processed data have been deposited in a public database such as GEO.

☒ Confirm that you have deposited or provided access to graph files (e.g. BED files) for the called peaks.

Data access links *May remain private before publication.*	https://www.ncbi.nlm.nih.gov/geo/query/acc.cgi?acc=GSE155882
Files in database submission	Raw and processed data for: scRNA/ATACseq, bulkRNAseq, PROseq, 4C and ChIPseq
Genome browser session (e.g. UCSC)	All bigwig files are available in GEO (GSE155882).

Methodology

Replicates	All transcriptional and epigenomic analysis were done in duplicates or triplicates.
Sequencing depth	- BulkRNAseq in cardiomyocytes: High-throughput sequencing was done using a PE75 run on a NextSeq 500 instrument (Illumina) for 9 samples - scRNAseq in non-cardiomyocytes: 8 samples were pooled and sequenced in one single lane on a NOVAseq (Illumina) - scATACseq in non-cardiomyocytes: 8 samples were pooled and sequenced in one single lane on a NOVAseq (Illumina) - PROseq in cardiac fibroblasts: 8 samples were pooled and sequenced SR75 bp in one single lane on a HiSeq 4000 (Illumina) - 4C: The 2 relevant samples were pooled with other 6 non-relevant samples using a SE75 run on a NextSeq 500 (Illumina) - ChIPseq: 6 relevant samples were pooled with other 6 non-relevant samples using a SE75 run on a NextSeq 500 (Illumina) -ChIPseq: 4 relevant samples were pooled with other 8 non-relevant samples using a SE75 run on a NextSeq 500 (Illumina)
Antibodies	Anti-HA antibody (Abcam #9110); H3k27ac (Abcam #ab4729)
Peak calling parameters	scATACseq: Raw sequencing reads were processed using the Cell Ranger ATAC v1.0 pipeline from 10X Genomics. In brief, reads were demultiplexed and aligned to the mouse mm10 genome. As a test of sample quality, a minimum of 70% of fragments overlapped targeted regions as defined by CellRanger. Peaks are then are called on aggregated fragments and then barcodes with fewer fragments than an automatically determined threshold (usually around 200) within these peaks are discarded. The remaining

fragments are counted to generate a peak-by-barcode matrix.

ChIPseq: Peaks were called using GEM14. Read counts per peak were generated with featureCounts15 and normalized to account for differences in sequencing depth between samples using upper quartile normalization separately for the ChIP and input sample.

Data quality

scATACseq: Raw sequencing reads were processed using the Cell Ranger ATAC v1.0 pipeline from 10X Genomics. In brief, reads were demultiplexed and aligned to the mouse mm10 genome. As a test of sample quality, a minimum of 70% of fragments overlapped targeted regions as defined by CellRanger. Peaks are then are called on aggregated fragments and then barcodes with fewer fragments than an automatically determined threshold (usually around 200) within these peaks are discarded. The remaining fragments are counted to generate a peak-by-barcode matrix.

ChIPseq:
Regions bound by MEOX1 and H3K27ac were determined using empirical Bayes F-tests for a quasi-likelihood negative binomial generalized log-linear model of the count data as implemented in edgeR. Specifically, we tested for a significant (i.e., non-zero at FDR < 5%) log2 fold-increase in normalized peak signal for ChIP versus the corresponding input sample. 6 samples (+ inputs) were ran for MEOX1 ChIP and only peaks present in minimum 2 out of 3 replicates were kept. 4 samples (+ inputs) were ran for H3K27ac ChIP. Region intersections were found using BEDTools16.

PROseq:
FastQ files resulting from the deep sequencing have been cleaned from low quality reads using Trimmomatic13. Trimmed FastQ files have been aligned together to the reference genome (mm10) using Bowtie2 (http://bowtie-bio.sourceforge.net/bowtie2/).

Software

scATAC: Raw sequencing reads were processed using the Cell Ranger ATAC v1.0 pipeline from 10X Genomics.

ChIPseq: Peaks were called using GEM14. Read counts per peak were generated with featureCounts. Region intersections were found using BEDTools16.

PROseq: All analysis have been run with Homer (4.11.1).